C. R. Palevol 16 (2017) 397–424

Contents lists available at ScienceDirect

Comptes Rendus Palevol

www.sciencedirect.com

General Palaeontology, Systematics and Evolution (Vertebrate Palaeontology)

Long bone histology of *Ophiacodon* reveals the geologically earliest occurrence of fibrolamellar bone in the mammalian stem lineage

*L'histologie d'os longs d'*Ophiacodon *révèle l'occurrence la plus précoce d'os fibro-lamellaire dans la lignée souche mammalienne*

Christen D. Shelton[a,b,*], Paul Martin Sander[b]

[a] *Department of Biological Sciences, University of Cape Town, Private Bag X3, Rondebosch, 7701 Cape Town, South Africa*
[b] *Division of Palaeontology, Steinmann Institute, University of Bonn, Nussallee 8, 53115 Bonn, Germany*

ARTICLE INFO

Article history:
Received 20 August 2016
Accepted after revision 2 February 2017
Available online 18 May 2017

Handled by Michel Laurin

Keywords:
Pelycosauria
Therapsida
Brinkman
Fibrolamellar bone

ABSTRACT

Shared histological characteristics have been observed in the bone matrix and vascularity between Ophiacodontidae and the later therapsids (Synapsida). Historically, this coincidence has been explained as simply a reflection of the presumed aquatic lifestyle of *Ophiacodon* or even a sign of immaturity. Here we show, by histologically sampling an ontogenetic series of *Ophiacodon* humeri, as well as additional material, the existence of fibrolamellar bone (FLB) in the postcranial bones of a pelycosaur. Our findings have reaffirmed what previous studies first described as fast growing tissue, and by proxy, have disproven that the highly vascularized cortex is simply a reflection of young age. This tissue demonstrates the classic histological characteristics of true FLB. The cortex consists of primary osteons in a woven bone matrix and remains highly vascularized throughout ontogeny, providing evidence for fast skeletal growth. Overall, the FLB tissue we have described in *Ophiacodon* is more advanced or "mammal-like" in terms of the osteonal development, bone matrix, and skeletal growth than what has been described thus far for any other pelycosaur taxon. With regards to the histological record, our results remain inconclusive as to the preferred ecology of *Ophiacodon* due to a similar cortical vascularity pattern exhibited by other carnivorous pelycosaurs. Our findings have set the

Abbreviations: BCBB, Briar Creek Bonebed; C, circumference; EC, erosional cavity; EFS, external fundamental system; Fm, formation; FLB, fibrolamellar bone; HL, hatching line; L, length; LAG, line of arrested growth; LB, lamellar bone; MC, medullary cavity; MR, medullary region; MOS, morphological ontogenetic stage; OL, osteocyte lacunae; PFB, parallel-fibered bone; RCBB, Rattlesnake Canyon Bonebed; RSC, Rattlesnake Canyon; SF, Sharpey's fibers; WB, woven bone; WPC, woven parallel-fibered complex.

* Corresponding author. Department of Biological Sciences, University of Cape Town, Private Bag X3, Rondebosch, 7701, Cape Town, South Africa.
E-mail address: martin.sander@uni-bonn.de (P.M. Sander).

http://dx.doi.org/10.1016/j.crpv.2017.02.002
1631-0683/© 2017 Académie des sciences. Published by Elsevier Masson SAS. All rights reserved.

evolutionary origins of FLB and high skeletal growth rates back approximately 20 million years to the Early Permian, and by phylogenetic extension perhaps the Late Carboniferous.
© 2017 Académie des sciences. Published by Elsevier Masson SAS. All rights reserved.

Mots clés :
Pélycosauriens
Thérapsidés
Brinkman
Os fibro-lamellaire

RÉSUMÉ

Il a été observé des caractéristiques histologiques partagées, dans la matrice et la vascularisation de l'os, entre les Ophiacodontidae et les thérapsidés (Synapsida) plus tardifs. Historiquement, cette coïncidence a été expliquée comme simplement un reflet du style présumé de vie aquatique d'*Ophiacodon*, ou même comme un signe d'immaturité. Ici est montrée histologiquement par l'échantillonnage des humérus d'une série ontogénétique d'*Ophiacodon*, ainsi que de matériel additionnel, l'existence d'os fibro-lamellaire dans les os post-crâniens d'un pélycosaure. Nos découvertes ont réaffirmé ce que des études antérieures avaient d'abord décrit comme tissu de croissance rapide ou par proxy, ont réfuté le fait que le cortex très vascularisé soit simplement un reflet du jeune âge. Ce tissu démontre les caractéristiques histologiques classiques d'un vrai os fibro-lamellaire (FLB). Le cortex est constitué d'ostéones primaires dans une matrice osseuse tramée et reste très vascularisé tout au long de l'ontogénie, fournissant la preuve d'une croissance osseuse rapide. Dans l'ensemble, le tissu FLB décrit chez *Ophiacodon* est plus avancé – ou de « type mammalien » – en termes de développement des ostéones, matrice osseuse et croissance du squelette, que ce qui avait été décrit, et de loin, pour tout autre taxon de pélycosaures. À propos de l'enregistrement histologique, nos résultats restent peu concluants en ce qui concerne l'écologie préférée d'*Ophiacodon*, en raison d'un *pattern* de vascularisation corticale similaire à celui d'autres pélycosaures. Nos découvertes placent les origines évolutives du FLB et les forts taux de croissance du squelette, à 20 Ma près, au Permien inférieur et, par extension phylogénétique, peut-être au Carbonifère.
© 2017 Académie des sciences. Publié par Elsevier Masson SAS. Tous droits réservés.

1. Introduction

1.1. Background

Ophiacodon (Marsh, 1878) is a basal synapsid that belongs to the clade Ophiacodontidae (Nopcsa, 1923) that existed between the Late Carboniferous and the Early Permian (Romer and Price, 1940). *Ophiacodon* is considered a more derived member of the clade, compared to, e.g., *Clepsydrops* (Laurin and de Buffrénil, 2016). Note that we use the term "pelycosaur" (paraphyletic) throughout this paper in an informal way and not as a clade name, to avoid using the cumbersome "non-therapsid synapsid".

Using a putative growth series of *Ophiacodon retroversus* (Fig. 1), Brinkman (1988) suggested that morphological ontogenetic stages (MOS) in pelycosaurs can be defined on the basis of degree of ossification of the limb bones. Size alone cannot be used as a proxy for reconstructing ontogenetic age in pelycosaur taxa because individuals of the same size may represent different stages of development. However, because of the delayed ossification observed in the epiphyses of *Ophiacodon* (Romer and Price, 1940), Brinkman was restricted as to what elements to use to test his hypothesis that the ossification of the limb bones is a better means of interpreting relative age of an individual than size. He chose the humerus because the complex articulations in the epiphyses exhibited more than two stages of ontogeny. We hypothesize that if the MOS of limb bones can be defined by degrees of ossification, then we should be able to relate MOS to bone histology.

Early histologic studies of *Ophiacodon* long bones, albeit based on scanty material, all concur that the histology contrasts in vascularity, matrix organization, and presence of growth marks from that observed in other pelycosaurs (Enlow, 1969; Enlow and Brown, 1957, 1958; de Ricqlès, 1974a,b). One explanation for these differences was an aquatic or amphibious lifestyle (Romer and Price, 1940) in *Ophiacodon*. Germain and Laurin (2005) tested this hypothesis by quantifying the global compactness of a complete transverse section and comparing it to that of extant animals. These authors advised caution when interpreting their results. Enlow (1969), however, noted that the characteristics of *Ophiacodon* bone tissue reflected fast skeletal growth, but he suggested this could just be the juvenile condition of his sample as adequate detailed ontogenetic comparisons were lacking for pelycosaurs.

Most recently, Laurin and de Buffrénil (2016) described the bone histology of the more basal ophiacodontid *Clepsydrops collettii* from a femur measuring 56.8 mm in length. This is one of the smallest femora on record for this species (Romer and Price, 1940; Shelton, 2015), but its small size may not necessarily indicate a juvenile (see above). Laurin and de Buffrénil (2016) compared the histology of the specimen to that of a femur of *O. uniformis* and noted that the cortex of *C. collettii* is much thinner, suggesting more of a terrestrial life style for the geologically earlier species. Additionally, Laurin and de Buffrénil (2016) found that *Ophiacodon* grew fast relative to extant squamates, and then found evidence of determinate growth in the form of an external fundamental system. Laurin and de Buffrénil

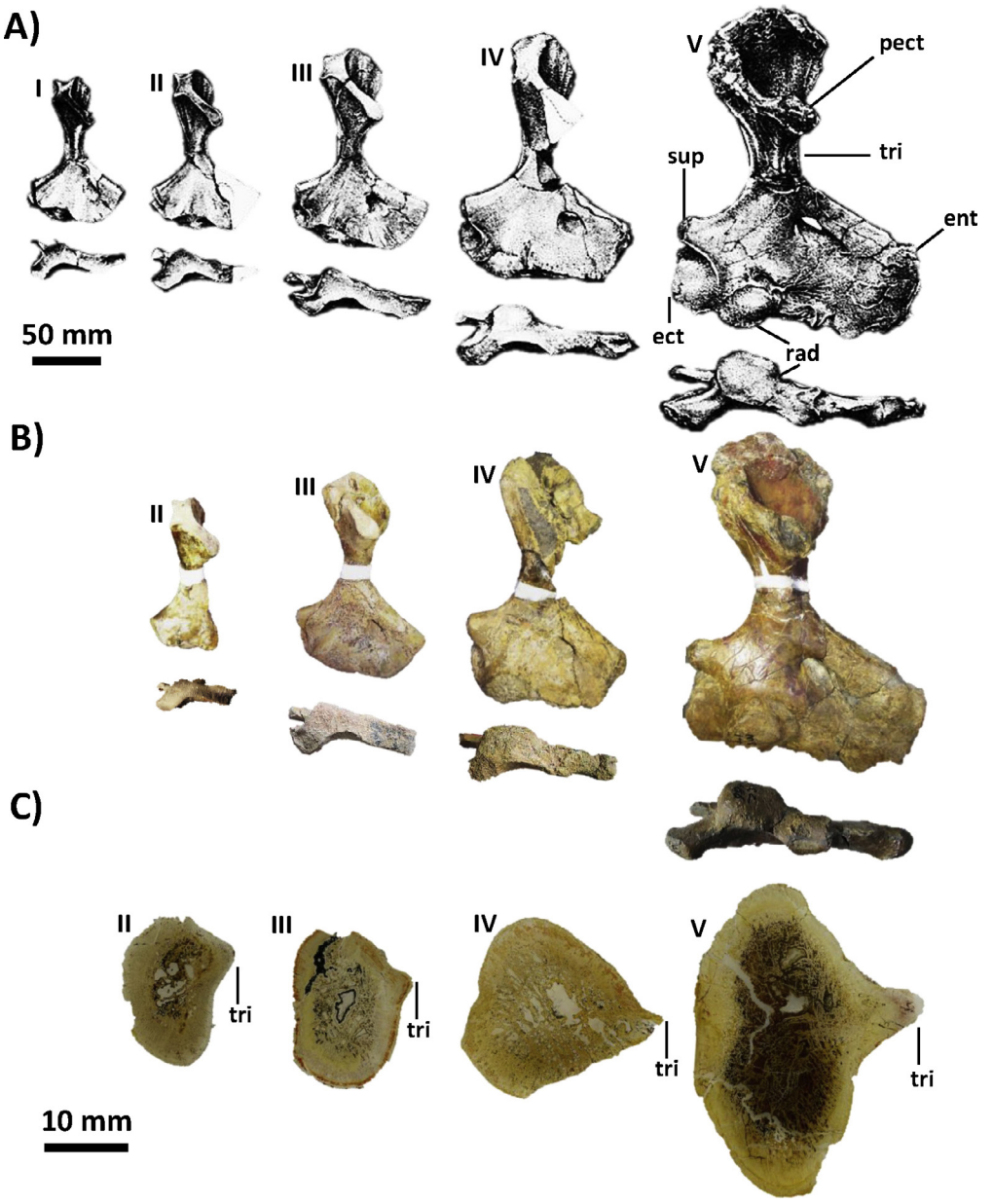

Fig. 1. Morphology and histology of ontogenetic series of *Ophiacodon* humeri figured by Brinkman (1988) and used in this study. A. Ontogenetic series of *Ophiacodon* humeri from the Rattlesnake Canyon locality in Archer County, Texas, from Brinkman (1988) illustrating his morphological ontogenetic stages (MOS) I to V. Each humerus is shown in ventral and distal view and is a right one except when noted otherwise. I = MCZ-1435, II = MCZ-5926, III = MCZ-2819 (reversed), IV = MCZ-4816 (reversed*), V = MCZ-1486. B. Photographs of the specimens figured by Brinkman (1988) with the exception of MCZ-1435 (MOS I), which was not available for this study. The white area in the mid-diaphysis represents the volume of bone sectioned for histological analysis and reconstructed with plaster. Each bone is shown in ventral and distal view. C. Corresponding sections from the mid-diaphysis of the four humeri of MOS II to V. Abbreviations: ect = ectepicondyle; ent = entepicondyle; pect = pectoralis crest; rad = radial articular surface; sup = supinator process; tri = triceps muscle insertion. *There are two humeri accessioned as MCZ-4816, a left and a right one. The left humerus is pictured here, but the image has been reversed to match the images in (A) reproduced from Brinkman (1988).

Fig. 1. Morphologie et histologie des humérus de la série ontogénétique d'*Ophiacodon*, figurés par Brinkman (1988) et utilisés dans cette étude. A. Humérus de la série ontogénétique d'*Ophiacodon* de la localité Rattlesnake Canyon, Archer County, Texas, d'après Brinkman (1988), illustrant les stades morphologiques ontogénétiques (MOS) I à V. Chaque humérus est présenté en vues ventrale et distale et est un humérus droit, sauf exception signalée. I = MCZ-1435, II = MCZ-5926, III = MCZ-2819 (retourné), IV = MCZ-4816 (retourné*), V = MCZ-1486. B. Photos des échantillons figurés par Brinkman (1988), à l'exception de MCZ-1435 (MOS I) qui n'était pas disponible pour cette étude. La zone blanche à mi-diaphyse représente le volume d'os sectionné en vue de l'analyse histologique et reconstitué par du plâtre. Chaque os est présenté en vues ventrale et distale. C. Sections correspondantes à mi-diaphyse pour les quatre humérus MOS II à V. Abréviations : ect = ectépicondyle ; ent = entépicondyle ; pect = crête pectorale ; rad = surface articulaire radiale ; sup = processus supinator ; tri = insertion du muscle triceps. *Il y a deux humérus MCZ-4816, un gauche et un droit. L'humérus gauche est figuré ici, mais l'image a été retournée pour correspondre à celles reproduites en (A) d'après Brinkman (1988).

(2016) interpreted the bone matrix in the deep cortex of their *Clepsydrops* femur as "woven-fibered", but the authors did not use the term fibrolamellar bone tissue (FLB) in that paper. Recently, Prondvai et al. (2014) redescribed FLB as a woven parallel-fibered complex (WPC). We choose to use the term FLB in this study because this is the more familiar one, but we agree with the conclusions of Prondvai et al. (2014).

Classically, FLB is defined as primary osteons, i.e., vascular canals filled in centripetally by lamellar bone, set in a matrix of woven bone, which can be identified by its non-birefringent properties in polarized light (Francillon-Vieillot et al., 1990). Additionally, FLB tends to be highly vascularized, and osteocyte lacunae in the woven bone matrix appear isometric ("plump"). More recently, FLB has been redefined based on its mode of osteogenesis (Prondvai et al., 2014; Stein and Prondvai, 2014) as a subcategory of the WPC. This kind of bone is formed by an initial scaffold of static osteoblasts (transforming into static, "plump" osteocytes) followed by dynamic osteogenesis filling in vascular spaces and leaving spindle-shaped, dynamic osteocytes behind (Prondvai et al., 2014; Stein and Prondvai, 2014). However, longitudinal sections are required in addition to transverse ones to reliably distinguish static from dynamic osteocytes based on their shape (Stein and Prondvai, 2014).

Ours is not the first study to investigate FLB in the long bones of a pelycosaur, however. Huttenlocker et al. (2006) and Huttenlocker and Rega (2012) suggested that FLB occurs in *Sphenacodon ferocior* (Synapsida: Sphenacodontidae). FLB was also reported in the elongate neural spines of sphenacodontids and edaphosaurids by Huttenlocker and Rega (2012), and Huttenlocker et al. (2010, 2011), but not in the long bones of these taxa.

1.2. Purpose of this study

In this study, we focus on the long bone histology of the basal synapsid *Ophiacodon* from Texas and Oklahoma localities of various ages in order to investigate what previous studies have called "fast growing" tissue as a possibly overlooked earliest occurrence of fibrolamellar bone in the lineage leading to mammals. Here, we have set out to histologically test the growth series hypothesis of Brinkman (1988) in which ontogenetic morphological stages in a taxon can be defined on the basis of degree of ossification of the limb bones because size alone is a poor proxy for estimating age in fossil taxa. For this, we specifically sectioned the *O. retroversus* humerus specimens studied by him. We compare the results to isolated *Ophiacodon* bones from various localities ranging in age from the Late Carboniferous to the Early Permian, with the aim of assigning them to ontogenetic stages. Because of the report by Enlow (1969), we expect to see histology that is similar to that observed by Shelton et al. (2013) in the long bones of *D. natalis* in which an incipient form of FLB was observed. Based on the earlier histological descriptions of *Ophiacodon* cortical bone (Enlow, 1969; Enlow and Brown, 1957, 1958; de Ricqlès, 1974a,b) and the high vascularity reported in these, we want to test the hypothesis that *Ophiacodon* has already evolved FLB compared to the pelycosaur *Dimetrodon*, which evolved an incipient form of FLB (Shelton et al., 2013). *Ophiacodon* is a geologically older synapsid than *Dimetrodon*, and generally is considered more basal (Benson, 2012; Kemp, 1987, 2007; Romer and Price, 1940). Previously, the earliest unequivocal occurrence of true FLB in Synapsida was found in the basal therapsid clade Dinocephalia (Reid, 1987; de Ricqlès, 1972; de Ricqlès, 1974a).

Institutional abbreviations: IPBSH, Palaeohistology collection, Steinmann Institute of Geology, Mineralogy, and Palaeontology, University of Bonn, Bonn, Germany; MCZ, Museum of Comparative Zoology, Harvard University, Cambridge, MA, USA; MSU, Geology Department, Midwestern State University, Wichita Falls, TX, USA; OMNH, Sam Noble Oklahoma Museum of Natural History, University of Oklahoma, Norman, OK, USA; UMMP, Museum of Paleontology, University of Michigan, Ann Arbor, MI, USA.

2. Materials

All material used in this study comes from a single genus, *Ophiacodon*, involving several species. The sample base for this study consists of a putative growth series of *O. retroversus* humeri from the RSC locality figured by Brinkman (1988), a single *O. uniformis* humerus, a single *Ophiacodon* sp. humerus, and four *Ophiacodon* femora from different localities (see Table 1). *Ophiacodon* humeri were identified by their enlarged entepicondyle and prominent supinator process. The femora have a prominent adductor crest that terminates in a sharp crest, and because of the lack of ossification the epiphyses are often concave (Reisz, 1986; Romer, 1956; Romer and Price, 1940).

The earliest bonebeds of rich vertebrate fauna come from the continental formations of the Wichita Group in Texas. In this study, we focus on the basal most Nocona Formation (Hentz, 1988), which is a consolidation of the Coleman Junction and Admiral Fms. as used by Romer (1974). Both the RCBB and the BCBB occur in this formation (Romer, 1974).

The Lower Permian *Ophiacodon* material from Southern Oklahoma is found in the Wellington and Garber formations, which are equivalent to the Upper Wichita and Lower Clear Fork Groups (Olson, 1967, 1977; Sander, 1989). This means that the Lower Permian *Ophiacodon* species from the Oklahoma deposits are geologically younger than those from the Texas ones. The oldest *Ophiacodon* material used in this study also comes from Oklahoma, specifically from the Upper Carboniferous beds of the Vamoose Fm. and the overlying Ada Fm. (Kissel and Lehman, 2002; Olson, 1977).

2.1. Ophiacodon humeri

2.1.1. Growth series of Ophiacodon humeri from RSC (Artinskian, Nocona formation)

We obtained permission for sampling of the specimens representing MOS II to MOS V of Brinkman (1988). These are specimens MCZ-5926, MCZ-2819, MCZ-4816, MCZ-1486 (Table 1; Fig. 1; Appendix 1A–E). MOS I, represented by humerus MCZ-1435 (Fig. 1A) could only be measured, but not histologically sampled. All specimens in Brinkman's (1988) study are of *O. retroversus*. Morphological

Table 1
Dimensions and growth mark count of the sectioned *Ophiacodon* long bones. Abbreviations: *C* = circumference; EFS = external fundamental system; *L* = length; MOS = morphological ontogenetic stage.
Tableau 1
Dimensions et comptage des marques de croissance dans les coupes d'os longs d'*Ophiacodon*. Abréviations : *C* = circonférence ; EFS = système fondamental externe ; *L* = longueur ; MOS = stage morphologique ontogénétique.

Specimen							Growth cycles	Estimated age (yr)	Observed LAGs	Geologic	
Number	Species	Bone	MOS	*L* (mm)	*C* (mm)	*L*/*C*				Age/Fm.	Locality in the USA
MCZ-5926	*O. retroversus*	Right humerus	II	76	44	1.73	1	1	0	L. Permian (Artinskian)/Nocona	Archer Co., TX
MCZ-2819	*O. retroversus*	Left humerus	III	97	50	1.94	2	2	1	L. Permian (Artinskian)/Nocona	Archer Co., TX
MCZ-4816	*O. retroversus*	Left humerus	IV	122	69	1.77	2	3	1	L. Permian (Artinskian)/Nocona	Archer Co., TX
MCZ-4816	*O. retroversus*	Right humerus	IV	125	71	1.76	2	3	1	L. Permian (Artinskian)/Nocona	Archer Co., TX
MCZ-1486	*O. retroversus*	Right humerus	V	152	83	1.83	4	16	4 (EFS)	L. Permian (Artinskian)/Nocona	Archer Co., TX
OMNH-73698	*Ophiacodon* (sp)	Right humerus	IV–V	113	50	2.26	2	Adult	EFS	Pennsylvanian/Vamoose	Seminole Co., OK
IPBSH-62	*O. uniformis*	Left humerus	V	82	37	2.22	3	Adult	2	L. Permian (Artinskian)/Nocona	Archer Co., TX
IPBSH-46	*Ophiacodon* (sp)	Right femur	NA	78	37	2.11	0	< 1	0	L. Permian (Artinskian)/Nocona	Archer Co., TX
OMNH-55234	*O. mirus*	Right femur	NA	100	60	1.67	3	?	2	U. Carboniferous/Ada	Seminole Co., OK
MSU Specimen	*O. uniformis*	Left femur	NA	115	55	2.09	8	?	4	L. Permian/Wellington	Jefferson Co., OK
OMNH-35389	*O. retroversus*	Left femur	NA	221	145	1.52	8	Adult	1 (EFS)	L. Permian/Garber	Tillman Co., OK

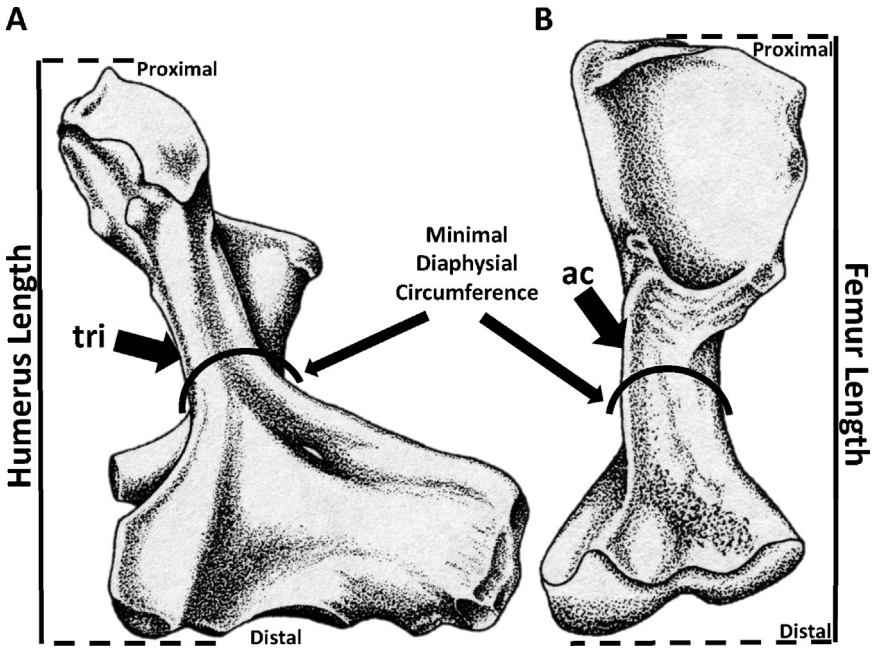

Fig. 2. Illustration of an *Ophiacodon retroversus* humerus (A) in dorsal view and a femur (B) in ventral view with indications of how and where the minimal diaphysis circumference (plane of section) and total length were measured. Arrows are pointing to muscle attachment sites. Abbreviations: ac = adductor crest, tri = triceps muscle insertion. (Modified from Reisz, 1986).
Fig. 2. Illustration d'un humérus (A) en vue dorsale et d'un fémur (B) en vue ventrale d'*Ophiacodon retroversus* ; on indique comment et où la circonférence minimale (plan de section) et la longueur totale de la diaphyse ont été mesurées. Les flèches pointent sur les sites d'attachement du muscle. Abréviations : ac = crête adductrice ; tri = insertion du muscle triceps. (Modifié d'après Reisz, 1986).

terminology is based on Romer and Price (1940) and Brinkman (1988).

2.1.2. Briar creek humerus

IPBSH-62: This left humerus pertains to *O. uniformis* (R. Reisz personal communication) and was obtained during a 2010 IPBSH excavation at the BCBB (Lower Permian, Artinskian, Nocona Formation) (Case, 1915; Hentz, 1988). A scapulocoracoid, probably of the same individual, was associated with this humerus. Based on the criteria of Brinkman (1988), this humerus is an early MOS V, even though unfinished bone is still present on the edge of the entepicondyle, the ectepicondyle, and the tip of the pectoralis process (Table 1; Appendix 1F). The ulnar and radial surfaces are both well ossified, and finished bone separates the pectoralis process from the proximal articular surface as defined by Brinkman (1988) for MOS V (see for example Fig. 1).

2.1.3. Seminole humerus

OMNH-73698: This right humerus is of *Ophiacodon* sp. and was collected in Seminole County, Oklahoma, from the Pennsylvanian Vamoose Formation. The specific site is OMNH-V1518, nicknamed the "Fixico Site" (Kissel and Lehman, 2002; Olson, 1977). It is difficult to assign a MOS to this humerus based on the criteria set by Brinkman (1988) because its distal end is damaged; however, what remains of the entepicondyle is highly rugose. The proximal end of the humerus is convex, and the pectoralis process is separated from the proximal articular surface by unfinished bone. Based on these observations, OMNH-73698 is a late MOS IV or early MOS V (Table 1; Appendix 1G).

2.2. Ophiacodon femora

OMNH-55234: This distal fragment of a right femur measures 100 mm in preserved length. The identification on the label as *O. mirus* is suspect due to the fragmentary nature of the bone. This specimen comes from the Upper Carboniferous Ada Formation, also in Seminole County, Oklahoma, from site OMNH-V1005, Site 4 (Table 1; Appendix 2B) (Kissel and Lehman, 2002; May et al., 2011; Olson, 1977).

OMNH-35389: This left femur is only identified as *Ophiacodon* sp. on the label and comes from the Lower Permian Garber Formation in Tillman County, Oklahoma, from OMNH-V716, Site 6 (Olson, 1967, 1977; Sander, 1989). Total length measures 221 mm (Table 1; Appendix 2D). Mostly due to the great size of this bone, but also after careful comparison to other *Ophiacodon* femora in collections and as described in the literature (Reisz, 1986; Romer and Price, 1940), OMNH-35389 most likely belongs to *O. retroversus*.

MSU uncatalogued: The only record accompanying this left femur is "Waurika Site", a well-known site in the Lower Permian Wellington Formation of Jefferson County, Oklahoma (Olson, 1977). The overall length of this bone measures 115 mm, and the mid-diaphyseal circumference is 55 mm. The adductor crest is damaged; thus, the circumference would have been larger in life. We identified the

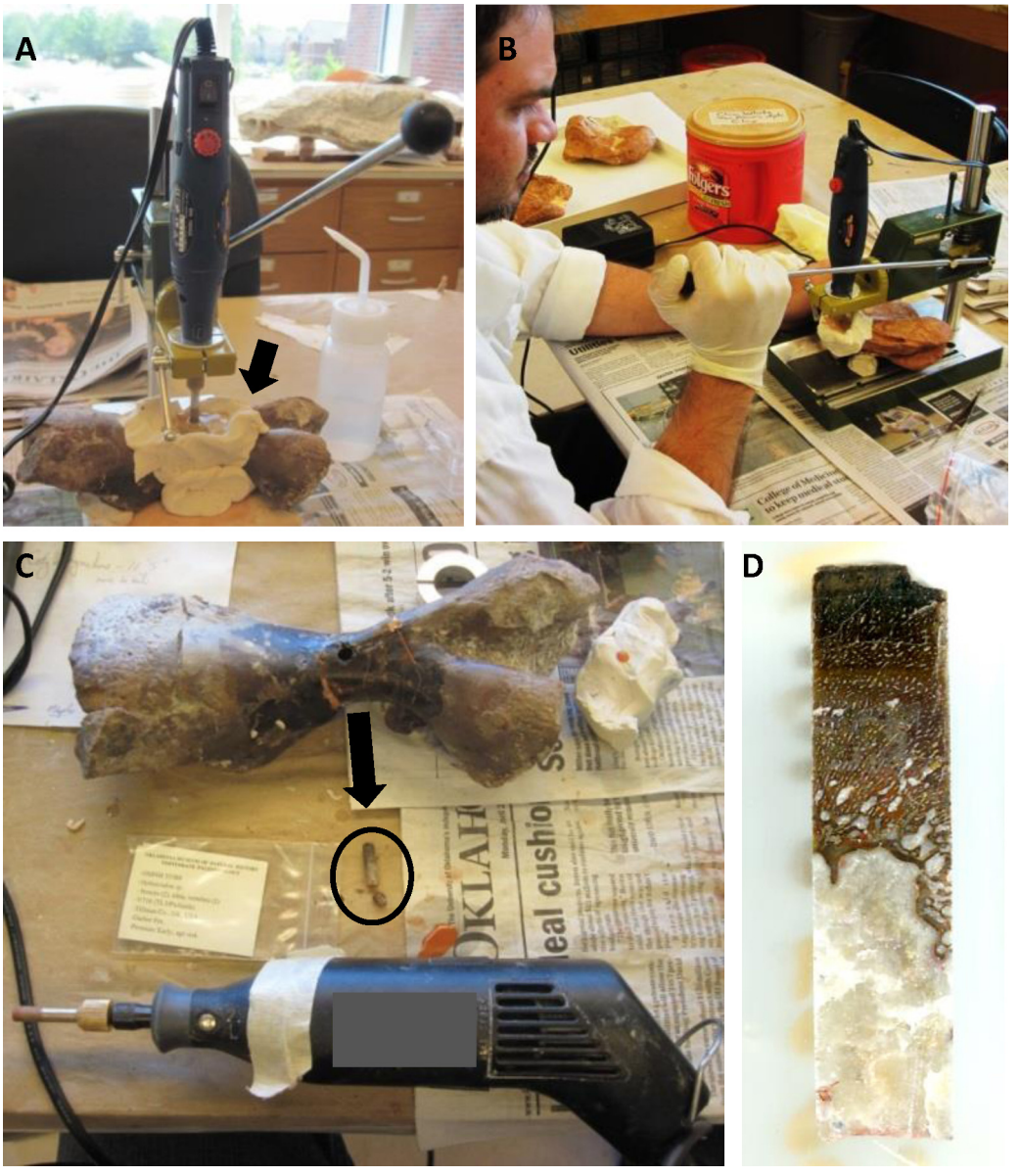

Fig. 3. Miniaturization of the coring process. A. The miniature hand-operated drill press is set up with a variable speed rotary tool. It is important to keep the core bit lubricated with water to prevent drill bit overheating. Arrow is pointing to a water bath constructed around the drilling site with plasticine. B. Operation of the drill press while drilling a pelycosaur bone. Light pressure is applied to the drill while in operation to facilitate a slow, steady pace. It is important to drill into the cortex slowly because the outer cortex may be sheared off if drilled too quickly. C. The results of the coring operation on femur OMNH-35389. The core was drilled on the dorsal side of the midshaft at the minimal diaphysis circumference. This core sample is further processed in the lab. Arrow is directed from drill site to the resulting core sample as indicated by the oval. D. The final core sectioned transversely after being embedded in a clear epoxy and before being processed into a petrographic thin-section (see Fig. 16).

Fig. 3. Miniaturisation du procédé de carottage. A. La presse miniature de forage à la main est installée avec un outil rotatif à vitesse variable. Il est important de maintenir la mèche lubrifiée par de l'eau pour éviter sa surchauffe. La flèche pointe sur un récipient d'eau construit autour du site de forage avec du plastique. B. Fonctionnement de la presse pendant le forage d'un os de pélycosaure. Une pression légère est appliquée pendant le forage pour faciliter une vitesse lente et constante. Il est important de forer lentement dans le cortex, car le cortex externe peut être arraché si le forage est trop rapide. C. Résultats du forage opéré sur le fémur OMNH-35389. Le forage a été exécuté sur la partie dorsale à l'endroit où la circonférence de la diaphyse est minimale. L'échantillon carotté est ensuite traité au laboratoire. La flèche est dirigée du site de forage vers l'échantillon carotté, ce qu'indique l'ovale. D. État final de la carotte sectionnée transversalement, avant d'être enrobée d'une résine époxy claire et avant d'être traitée pour en obtenir une section mince pétrographique (voir Fig. 16).

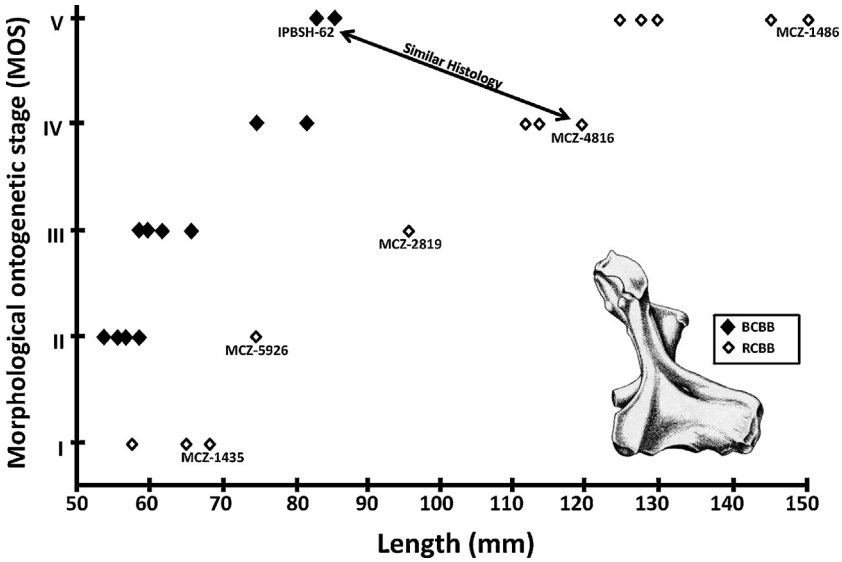

Fig. 4. Graph showing the relationship between size and MOS of *Ophiacodon* humeri from the Briar Creek Bonebed (black diamonds) and other localities (open diamonds) from the Petrolia and Nocona formations. The latter includes the sectioned Rattlesnake Canyon humeri. These humeri, as well as IPBSH-62, are labeled on the graph. The remaining data points cannot be marked because Brinkman (1988) did not identify specimens used in the plot. Note the arrow indicating that IPBSH-62 (MOSV) and MCZ-4816 (MOS IV) both have a similar histology with the exception of better developed primary osteons in MCZ-4816. Graph is inverted and modified from Brinkman (1988, fig. 7).

Fig. 4. Graphique montrant la relation entre taille et stade morphologique ontogénétique (MOS) des humérus d'*Ophiacodon* de Briar Creek Bonebed (losanges noirs) et d'autres localités (losanges blancs) des formations Petrolia et Nocona. La dernière inclut les humérus sectionnés de Rattlesnake Canyon. Ces humérus ainsi que IPBSH-62 sont reportés sur le graphique. Les points restants ne peuvent être marqués, car Brinkman (1988) n'a pas identifié les échantillons utilisés dans le graphique. À noter la flèche indiquant que IPBSH-62 (MOS V) et MCZ-4816 (MOS IV) ont une histologie similaire, exception faite d'ostéones primaires mieux développées en MCZ-4816. Le graphique est inversé et modifié d'après Brinkman (1988, fig. 7).

specimen as *O. uniformis* based on Romer and Price (1940) and Reisz (1986) (Table 1; Appendix 2C).

IPBSH-46: This right femur was obtained during the 2011 excavation of the authors at the BCBB (Lower Permian, Artinskian, Nocona Formation). The total length is 78 mm. Based on this criterion alone, we would have identified this specimen as *O. uniformis* (Romer and Price, 1940; Brinkman, 1988) (Table 1; Appendix 2A). However, the small size of the specimen together with the simple morphology of the little developed distal condyles suggests that the femur belongs to a very immature individual of a larger species. For our purposes, we simply identify it as *Ophiacodon* sp. due to the early ontogenetic stage. The only other contemporaneous *Ophiacodon* species was the larger *O. retroversus*, which is known from Artinskian bone beds.

3. Methods

3.1. The full mid-diaphysis cross-sectioning method

The mid-diaphysis is the region of a long bone where the most complete record of growth is preserved. It also corresponds to the area of the smallest shaft circumference (Currey, 2002; Francillon-Vieillot et al., 1990). Silicon molds (Provil NovoTM putty, Heraeus Kulzer Technique) of all long bone diaphyses were created before sectioning to record the original shape of the shaft region and aid in later reconstruction of the specimen. To prevent splintering of the outer cortex during sectioning, the region to be sectioned was encased in an epoxy resin putty (Technovit Universal TM liquid and Technovit TM 5071 powder, Heraeus Kulzer Technique). After curing of the putty, the bone was sectioned transversely in two cuts with a rock saw equipped with a standard diamond-tipped blade, removing a slice of the diaphysis. Only two specimens (IPBSH-62 and IPBSH-46), excavated by the authors, were sectioned longitudinally as loaned specimens were only allotted for transverse sectioning. Humeral midshaft sections bisect the area where the medial head of the triceps muscle inserts, giving the cross-section a distinct shape (Fig. 2A). Femoral sections bisect the area of the adductor muscle attachment (Fig. 2B) (Romer, 1956; Romer and Price, 1940). After removal of the bone slice, the epoxy resin putty was dissolved with acetone, and the bone was reconstructed by filling in the mold with plaster, thus preserving the morphological and anatomical features of the original material. After sawing, bone sections were ground to approximately 35 to 50 μm by hand on a glass plate with wet grit (600 and 800) and sealed with a cover slip using UV activated resin (Verifix TM LV 740, Bohle). The following specimens were sectioned using this method: MCZ-5926, MCZ-2819, MCZ-4816, MCZ-1486, and IPBSH-62 (all humeri) and OMNH-55234, IPBSH-46, and the MSU uncatalogued (all femora).

3.2. The miniaturized coring method

This method is a miniaturized version of the coring method for histological sampling described by Stein and Sander (2009). While a full cross-section of the

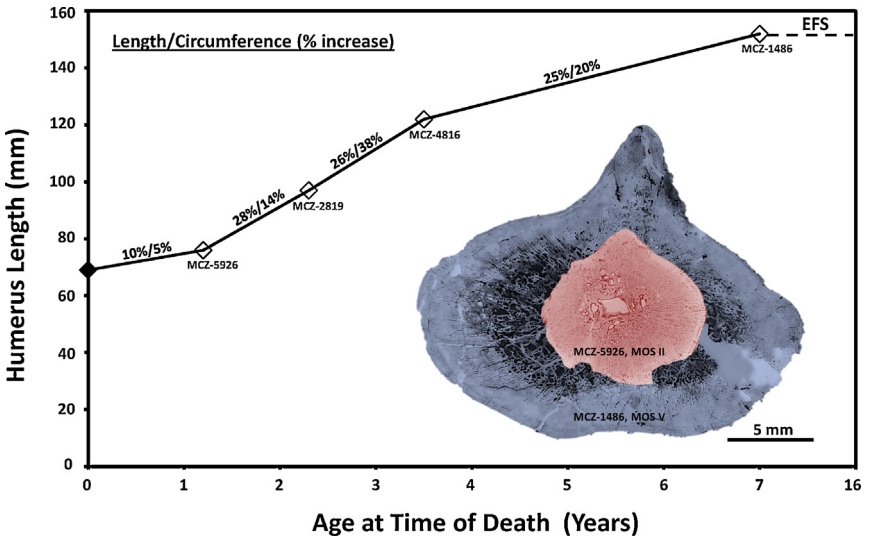

Fig. 5. *Ophiacodon retroversus* growth curve, with specimens representing each MOS, constructed by plotting overall bone length and individual age at time of death for each humerus. Age was calculated by correlating subsequent overlays of each MOS and matching successive cycle boundaries, resulting in an asymptotic growth curve. MCZ-1435, MOS I, (length 69 mm and circumference 42 mm) was included as the earliest morphological stage of the ontogenetic series (black diamond); however, it could not be sectioned. Based on the histology of the next larger specimen, we assumed that the bone is from a young animal less than one year old that died shortly after hatching. All other humeri represented by white diamonds were sectioned and recorded in Table 1. Included here is the percentage increase of length and minimal diaphysis circumference between each successive MOS. Length seems to increase steadily throughout ontogeny, but circumference increases quite rapidly, peaking at 38 percent between MOS III and MOS IV. MCZ-5926 (MOS II) is a humerus from an individual that died shortly after completing its first year of life marked by an annulus. The hatching line is still visible in the deep cortex, but was destroyed by resorption in the higher MOS. MCZ-1486 (MOSV) contains many LAGs but no annuli, which correspond to the slowed growth. This is also evident by the reduction of vascularization and the presence of an external fundamental system (EFS) in the outermost cortex. The EFS indicates that this individual had reached skeletal maturity and lived at least for another eight years.

Fig. 5. Courbe de croissance d'*Ophiacodon reversus*, avec les spécimens représentant chacun des MOS, construite en reportant la longueur totale et l'âge de l'individu au moment de sa mort, dans le cas de chaque humérus. L'âge a été calculé en corrélant les recouvrements subséquents de chaque MOS et en comparant les limites entre cycles successifs, ce qui résulte en une courbe de croissance asymptotique. MCZ-1435, MOS I (longueur 69 mm et circonférence 42 mm) a été inclus dans le stade morphologique le plus précoce de la série ontogénétique (losange noir) ; cependant, il n'a pu être sectionné. En nous basant sur l'histologie de l'échantillon suivant, plus grand, nous présumons que l'os appartient à un animal jeune, de moins d'un an, qui est mort peu de temps après l'éclosion. Tous les autres humérus représentés par des losanges blancs ont été sectionnés et sont répertoriés dans le Tableau 1. Est aussi inscrite l'augmentation de longueur et de circonférence minimale de la diaphyse en pour cent, entre les MOS successifs. La longueur semble augmenter de manière régulière au cours de l'ontogénie, mais la circonférence augmente rapidement, avec un pic à 38 % entre MOS III et MOS IV. MCZ-5926 (MOS II) est l'humérus d'un individu, mort peu de temps après sa première année, comme le montre l'annulus. La ligne d'éclosion est encore visible dans le cortex profond, mais a été détruite par la résorption du MOS plus haut. MCZ61486 (MOS V) contient de nombreuses LAGs (lignes de croissance arrêtée), mais pas d'annulus, ce qui correspond à la croissance ralentie. Ceci est également évident du fait de la réduction de la vascularisation et de la présence d'un système fondamental externe (EFS) dans le cortex le plus extérieur. L'EFS indique que cet individu a atteint la maturité squelettique et a vécu au moins encore huit ans.

mid-diaphysis is preferred, coring increases sample size and permits access to more valuable specimens and those encased in large aggregations of matrix. It is crucial for the coring method that homologous locations are sampled in the different bones (Stein and Sander, 2009). Material available for sampling while onsite at the OMNH was core drilled dorsally at the mid-diaphysis, as the growth marks in this region are better visible, allowing for minimal damage to the specimen (humerus OMNH-73698 and femur OMNH-35389) (Appendix 1G and 2D). The direction of the bone long axis was marked on the bone surface at the sample location by a line so that sample orientation could be maintained. Two sizes of diamond-tipped coring bits were used (3 mm and 5 mm), and attached to a Dremel-type variable speed rotary tool mounted on a hand-operated miniature drill press. Water was used to lubricate the drill bit to reduce friction and prevent damage of the outer periosteal tissue. The lubricant water was contained by building a small reservoir using plasticine (Fig. 3A). The core hole was later infilled with plasticine.

Cores were thin-sectioned in the Steinman Institute's paleohistology laboratory. Each core was imbedded in a translucent Araldite 2020 epoxy resin (Bodo Möller Chemie) and allowed to harden for 24 hours before being sectioned by cutting the core perpendicular to the long axis of the original long bone orientation (Fig. 3), as indicated by the mark drawn prior to coring. The plane of section is comparable to the full transverse section of the mid-diaphysis. Sectioning and slide preparation follow the same procedure as that described above for bones cut in full cross-section.

Petrographic thin-sections were imaged in normal transmitted light and polarized transmitted light using a Leica DM2500LP Polarizing Microscope configured with a 360 degree rotating stage and polarizing and lambda filters. Digital images were acquired with a Leica DFC420 color camera and processed using the 2007 Leica IMAGE ACCESS EASYLAB 7 software (Leica, Wetzlar, Germany; see Petermann and Sander, 2013). No further editing beyond adding the scale to the image was done in the

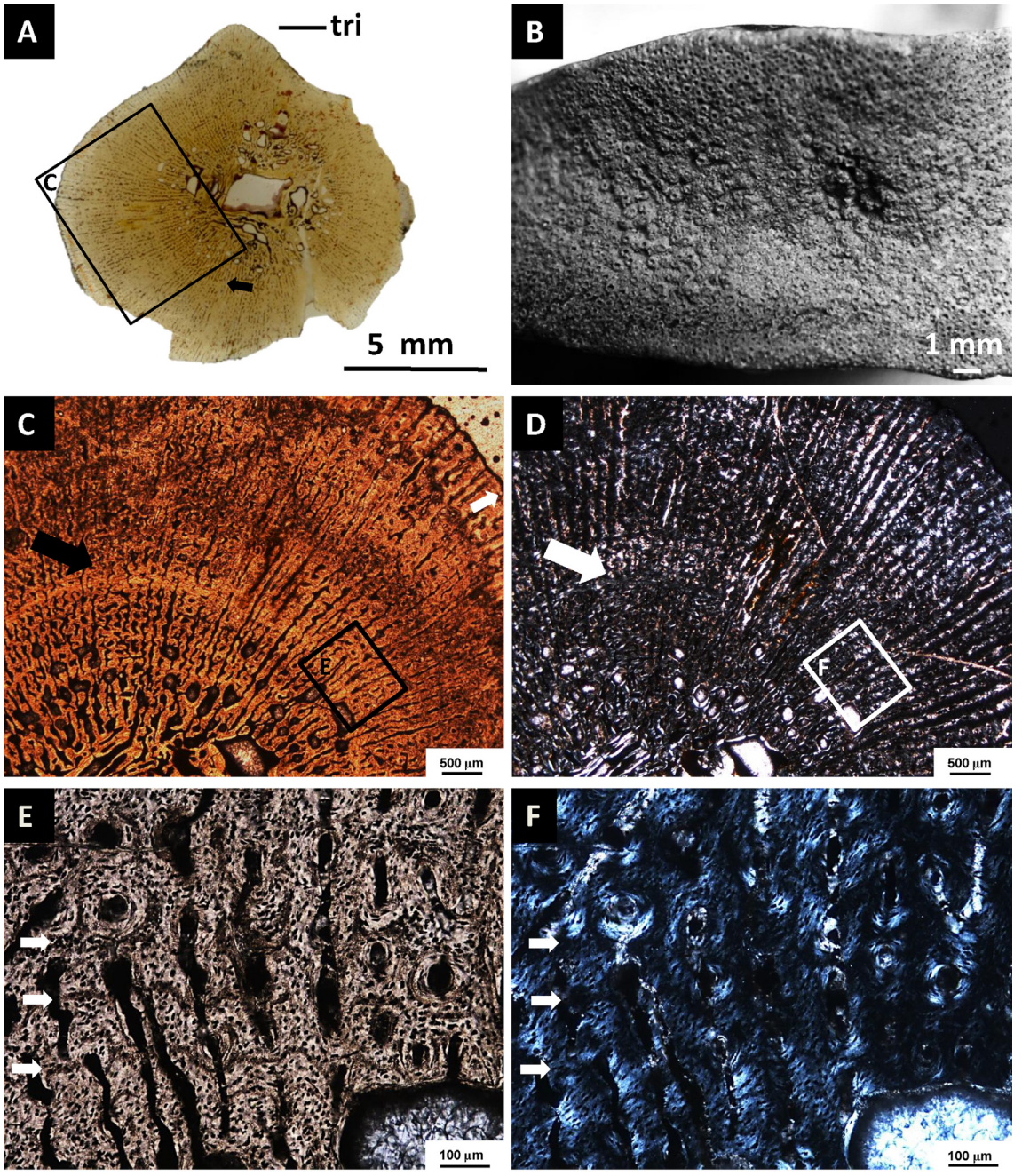

Fig. 6. Humerus MCZ-5926, MOS II, of *O. retroversus*. A. Scan of transverse section through the mid-diaphysis in normal lig ht. Notice the "bicycle wheel" pattern formed by the radial arrangement of the vascular canals. Note that the radial canals are in the plane of section and extend from the medullary cavity to the outer cortex. The medullary cavity is occluded with mostly secondary (some primary) trabeculae, and erosional cavities (EC) are present in the medullary margin area. Note that EC do not extend past the hatching line (HL) (indicated by arrow), which is a line of slowed growth marking the time of hatching, forming the boundary between the pre-hatching embryonic bone inside, and the post-hatching periosteal bone beyond. Also, the size of the vascular canals is larger in the pre-hatching area and smaller in the post-hatching area. B. Close-up of the distal epiphysis with exposed calcified cartilaginous tubules. C. Photomicrographs of the mid-diaphyseal cortex viewed in normal transmitted light magnified from an area marked by a box in (A). The large arrow indicates the HL. Note the two pre-hatching growth marks just beyond the medullary cavity. The small arrow indicates the line of arrested growth approximately three millimeters beyond the HL. D. Same view as in (C) but in polarized transmitted light. Vascular canals are more distinctive in polarized light. The "bicycle wheel" pattern is very prominent caused by the birefringence of lamellar bone. Also, EC are clearly distinguishable. Parallel-fibered and woven bone matrix are found throughout the cortex. The arrow indicates the position of the HL. E. Microscopic close-up of the HL indicated by the boxed area in (C) in normal transmitted light. Notice the three closely spaced growth marks within the HL (indicated by arrows). At MOS II, EC have not yet crossed the HL. Note the plump shape and high density of the osteocyte lacunae. F. Same view as in (E) but in polarized transmitted light. Note the mix of incipient and fully formed primary osteons set in a woven bone matrix, thus forming fibrolamellar bone. Abbreviation: tri = triceps muscle insertion.

software. Overview images of petrographic thin-sections were obtained in normal light with an EPSON V750 high-resolution transmitted light scanner. This is a faster and easier method compared to electronically stitching together many small microscopic images if polarized light images are not required. Bone histological terminology follows Francillon-Vieillot et al. (1990) and Shelton et al. (2013).

Petrographic slides are reposited at the IPBSH. Additionally, sections of all MCZ and OMNH material are deposited at those institutions.

3.3. Measurements

It is crucial to perform morphometric analysis of the individual bone being sampled preceding any histological work to procure the raw metric data before the bone is damaged in any way (e.g., Klein and Sander, 2007; Sander and Klein, 2005; Sander et al., 2006). Total length and minimal diaphysis circumference was recorded for each bone using standard analytical calipers and a metric measuring tape (Table 1). Length was taken as the total distance between the termination of the proximal and distal ends. Circumference was taken at the mid-diaphysis (see Fig. 2). The ratio of the length to circumference was also calculated to evaluate interspecific variation (Table 1).

3.4. Skeletochronological analysis

Brinkman's humeral growth staging (Fig. 1) was used to construct a semi-quantitative composite growth curve plotting MOS against size (Fig. 4). Each cross-section was hand-drawn with a camera lucida and then traced onto clear translucent sheets. Subsequent overlays were correlated by matching cycle boundaries of successive MOS. This allowed for age estimates of the individual specimens at time of death, and the results are quantified in a growth curve (Fig. 5). This method is similar to that described by Bybee et al. (2006) to reconstruct growth curves from *Allosaurus* bones. Note that MCZ-1435, MOS I, (length 69 mm and circumference 42 mm) was included in this growth curve as the initial data point, but it was not available for sectioning.

4. Results

4.1. Morphometry

Length and circumference data for each bone used in this study is presented in Table 1. The average length to circumference (L/C) ratio of the sampled *Ophiacodon* humeri was 1.96 and for the femora was 1.91 (Table 1). However, the L/C ratio of the MOS V humerus from RSC (MCZ-1486) is different from the L/C ratio of the BCBB humerus (IPBSH-62) of the same stage. MCZ-1486 is 152 mm in length and 83 mm in circumference with a ratio of 1.83 (Table 1). IPBSH-62 is 82 mm in length and 37 mm in circumference with a ratio of 2.22. The RSC humerus is 46% longer and the circumference is 55% larger than the BCBB humerus.

4.2. Ophiacodon humerus histology

The histology of all transversely sectioned humeri (Table 1) is described below by increasing MOS. All histology is described from the mid-diaphyseal section bisecting the triceps muscle insertion, a prominent feature in *Ophiacodon* (Romer, 1956) (Figs. 1 and 2).

4.2.1. Brinkman's ontogenetic series of RSC *O. retroversus humeri*

4.2.1.1. Histology of MCZ-5926 (MOS II). MCZ-5926 (Figs. 1 and 4) is a right humerus 76.2 mm in length (Appendix 1A) with unfinished epiphyses exhibiting small vascular canals extending into the endochondral bone (Fig. 6B) and a smooth diaphyseal cortical surface. In transverse section, the midshaft cortex is relatively thick and consists of parallel-fibered bone (PFB) and woven bone (WB), prevalent dorsally and ventrally. Vascularization in the cortex is dense and consists of longitudinal and radial canals. In the dorsal and ventral regions of the outermost cortex, anastomosis is strongest between the longitudinal canals, making the vascularity more of a reticular pattern in this area. The overall radial organization of the canals gives the cortical bone a "bicycle wheel" pattern (Fig. 6C and D). The vascular canals have varying degrees of lamellar bone (LB) infilling. Some have none while others are immature to fully formed primary osteons (Fig. 6E and F). By definition (Francillon-Vieillot et al., 1990), the combination of primary osteons set in a woven bone matrix identifies this

Fig. 6. Humérus MCZ-5926, MOS II d'*O. reversus*. A. Scan d'une section transverse à mi-diaphyse en lumière normale. À noter le *pattern* en « roue de bicyclette » formé d'un arrangement radial des canaux vasculaires. À noter que les canaux radiaux sont dans le plan de section et s'observent de la cavité médullaire jusqu'au cortex externe. La cavité médullaire est obstruée par des trabeculae surtout secondaires (quelques-uns sont primaires) et des cavités d'érosion (EC) sont présentes dans la zone de bordure médullaire. À noter que les EC ne se développent pas au-delà de la ligne d'éclosion (HL) – comme indiqué par la flèche –, qui est une ligne de croissance lente marquant le temps d'éclosion, formant la limite entre l'os embryonnaire pré-éclosion, à l'intérieur, et l'os périostéen post-éclosion, au-delà. La taille des canaux vasculaires est aussi plus grande dans la zone de pré-éclosion et plus petite dans la zone de post-éclosion. B. Fermeture de l'épiphyse distale avec des tubules cartilagineux calcifiés externes. C. Microphotos du cortex à mi-diaphyse en lumière transmise normale à partir d'une zone encadrée en (A). La flèche large indique l'HL. À noter les deux marques de croissance pré-éclosion juste au-delà de la cavité médullaire. La petite flèche indique la ligne de croissance arrêtée, approximativement 3 mm au-delà de l'HL. D. Même vue qu'en (C), mais en lumière transmise polarisée. Les canaux vasculaires se distinguent mieux en lumière polarisée. Le *pattern* en « roue de bicyclette » est frappant, en raison de la biréfringence de l'os lamellaire. Les EC se distinguent également de manière nette. Une matrice osseuse tramée et fibro-lamellaire est mise en évidence au sein du cortex. La flèche indique la position de l'HL. E. Fermeture observée au microscope de l'HL, indiquée par la zone encadrée en (C), en lumière transmise normale. À noter les trois marques de croissance peu espacées au sein de l'HL (indiquées par des flèches). À MOOS II, les EC n'ont pas traversé l'HL. À noter la forme dodue et la forte densité des lacunes d'ostéocytes. F. Même vue qu'en (E), mais en lumière transmise polarisée. À noter le mélange d'ostéones primaires naissantes et complètement formées dans une matrice osseuse tramée, donc formant de l'os fibro-lamellaire. Abréviations : tri = insertion du muscle triceps.

tissue as fibrolamellar bone (FLB). Osteocyte lacunae (OL) are plump to sub-angular and appear to be randomly oriented in between the osteons, while others that follow the circumferential layering of the LB are flat.

The cortical bone contains a record of cyclical growth. Most notable is the division of the cortex by a feature we interpret as being a putative hatching line (HL) (Fig. 6A and C) into a pre-hatching and a post-hatching part (Rogers et al., 2016). The HL indicates the time when the animal emerged from an amniotic egg. The HL appears as an annulus with three corresponding lines of arrested growth (LAGs), indicating a period where growth slowed down dramatically (Fig. 6E and F). The embryonic bone inside the HL differs sharply from the tissue laid down subsequently. The width of the vascular canals inside the HL is greater and more irregular than beyond the HL. The bone matrix is exclusively woven bone. Two indistinct cycles of slowed growth can be seen within the embryonic bone. These obviously formed while the animal was *in ovo*, but the significance of these growth marks is unknown. The HL has a circumference of about 20 mm. One LAG appears near the outer bone surface in the post-hatching bone, approximately 3 mm beyond the HL (Fig. 6C). Sharpey's fibers (SF) were not observed. This animal died very shortly after completing its first year of life (Fig. 5).

The medullary and pre-hatching regions are distinguished from the post-hatching region of the cortex by small to medium-sized erosional cavities (EC), some of which are lined by a thin layer of lamellar bone. Endosteal lamellar bone is present in the form of mostly secondary trabecular bone in the medullary cavity, but there are also some primary trabeculae.

4.2.1.2. Histology of MCZ-2819 (MOS III). MCZ-2819 (Figs. 1 and 4) is a left humerus 97.22 mm in length with unfinished epiphyses (Appendix 1B). The small vascular canals extending into the endochondral bone (first observed in MCZ-5926, MOS II) are only visible as darkened rings on the proximal articular surface (not pictured). The outer cortical surface of the bone is also smooth. In the transverse section, PFB is prevalent on the posterodorsal side, as well as in the outermost cortex at the triceps muscle attachment. WB is seen throughout the cortex, especially surrounding the vascular canals. Vascularity consists of some radial canals but mostly small longitudinal canals from the mid to outer cortex, and the "bicycle wheel" pattern persists (Figs. 7A and B). In the deeper cortex, vascularity is more radial and canals are more open (Fig. 7C). The vascular canals have varying degrees of LB infilling; they are thus incipient to fully formed primary osteons (Fig. 7B). OL are plump to sub-angular as well as flat and oriented parallel to the bone surface in the slower growing tissue.

The cortical bone contains two cycle boundaries (Table 1) marked by annuli. The most recent cycle is visible in the darkly stained area of the outer cortex (Fig. 7F). The HL is no longer visible as it has been removed by the advancing resorption front. SF are located mostly on the anterior side and visible at the triceps muscle attachment (Fig. 7B). The deepest LAG in MCZ-2819 (Fig. 7E and F) correlates with the most superficial LAG in MCZ-5926; therefore, we presume that MCZ-2819 died shortly after the second year of life (Fig. 5).

The medullary cavity is occluded by a network of secondary trabeculae. ECs with a lining of lamellar bone are abundant, having formed by expansion of the medullary cavity, altering the pre- and hatching areas observed in humerus MCZ-5926 (Fig. 6). Small to medium-sized ECs mark the outermost boundary of the medullary region (Fig. 7C and D).

4.2.1.3. Histology of MCZ-4816 (MOS IV). MCZ-4816 (Figs. 1 and 4) consists of a pair of associated humeri that presumably came from the same individual (Appendix 1C and D). Both are damaged at the mid-diaphysis, the right humerus is encrusted with a hematitic or limonitic matrix, which incorporates additional small bones (Fig. 8A and B). The two humeri themselves look yellowed and weathered with a worn surface. Epiphyses look roughened and black. The left humerus, which was figured by Brinkman (1988), has a length of 122 mm, and the right humerus is 125 mm (Table 1). Histology of the two humeri is identical, reaffirming that they are from the same individual, and will be described together. Unfortunately, preservation of the histology is not optimal (Fig. 8C and E); most of the histological detail has been lost due to the effects of weathering and diagenesis. Diagenetic staining has darkened the tissue, making LAGs, OL, and even bone matrix nearly impossible to distinguish. LB can still be seen infilling some of the vascular canals. However, immature or fully formed primary osteons cannot be differentiated (Fig. 8E and F); the canals appear ragged and degraded taphonomically (Fig. 8C). The "bicycle wheel" vascularity pattern is still visible in the cortex (Fig. 8D). PFB is distinguishable in some patchy areas. WB could not be observed. Vascularity appears to consist of small densely concentrated radial and longitudinal canals. The outermost cortex has even thinner radial canals.

The preserved growth record consists of two cycle boundaries (Table 1) marked by annuli within the medullary region and inner cortex, mostly visible in polarized light (Fig. 8D). By overlaying the earliest annulus with the second growth mark of MCZ-2819, this animal is estimated to have died between the third and fourth year of life (Fig. 5).

The medullary margin consists mainly of large ECs stretching into the cortex as they appear to follow the orientation of the vascular network. Interstitial primary cortical bone is incorporated as trabeculae due to the formation of large and small EC lined by lamellar bone (Fig. 8C and D).

4.2.1.4. Histology of MCZ-1486 (MOS V). MCZ-1486 (Figs. 1 and 4) is a right humerus 152 mm in length with fully ossified epiphyses (Appendix 1E). The outer surface is smooth with much rugosity in the epiphyses. In the midshaft petrographic section, the cortical bone is thin (Fig. 9A and C) and vascularized by radial and radially arranged longitudinal canals, again forming the "bicycle wheel" pattern (Fig. 9C, D, E). WB is concentrated in the dorsal and posterior areas. PFB is seen throughout the cortex. Dark SF appear in the anterior region. OL are

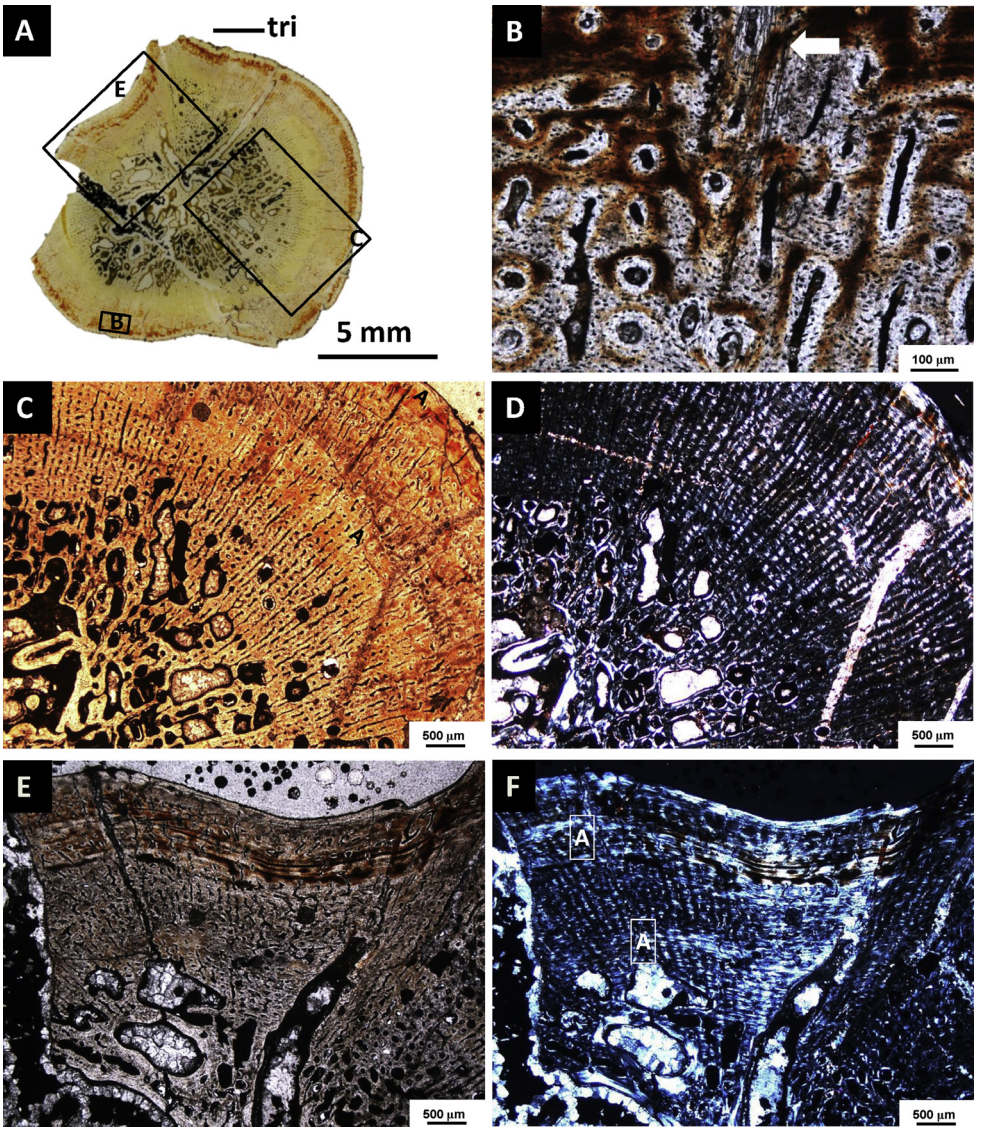

Fig. 7. MCZ-2819, MOS III, *O. retroversus* humerus. A. Scan of transverse section through the mid-diaphysis in normal light. The HL has been completely resorbed by expansion of the medullary cavity. Radial and longitudinal vascular canals remain consistent with the "bicycle wheel" pattern. The EC have greatly increased throughout the medullary margin. Growth marks are preserved in the darkly iron-stained areas of the cortex. B. Photomicrograph of the outer cortex in normal transmitted light. Arrow points to Sharpey's fibers. C. Microscopic view of the mid-diaphysis cortex in normal transmitted light. Note that the expansion of the medullary cavity has erased all traces of the pre-hatching bone. Also, the vascular canals appear to decrease in size towards the outer cortex. The approximate location of the two annuli are denoted by the letter "A". D. Same view as (C) but in polarized transmitted light. The "bicycle wheel" pattern is better visible given the extinction pattern of the lamellar bone infilling in contrast to the woven bone matrix. E. Microscopic view of the outer cortex in normal transmitted light. The darker iron-staining preserved growth marks just below the cortical surface, marking the end of the second growth cycle in the *Ophiacodon* humeral growth series. F. Same view as (E) in polarized transmitted light. Note the inner annulus of the first year growth cycle. Also the annulus corresponding with the visible growth marks in (E) marks the second year growth cycle. Abbreviations: A = annulus; tri = triceps muscle insertion.

Fig. 7. Humérus MCZ-2819, MOS III d'*O. retroversus*. A. Scan de section transverse à mi-diaphyse en lumière normale. L'HL a été complètement résorbée par l'expansion de la cavité médullaire. Les canaux vasculaires longitudinaux et radiaux restent compatibles avec le *pattern* « roue de bicyclette ». Les EC ont beaucoup augmenté dans la bordure médullaire. Les marques de croissance sont préservées sous forme de zones assombries par leur coloration par le fer. B. Microphoto du cortex externe en lumière transmise normale. La flèche pointe sur les fibres de Sharpey. C. Vue microscopique du cortex à mi-diaphyse en lumière transmise normale. À noter que l'expansion de la cavité médullaire a effacé toute trace de l'os pré-éclosion. Les canaux vasculaires apparaissent avec une taille décroissante vers le cortex externe. La localisation approximative des deux annuli est indiquée par la lettre « A ». D. Même vue qu'en (C), mais en lumière transmise polarisée. Le *pattern* en « roue de bicyclette » est plus visible, étant donné le *pattern* d'extinction du remplissage d'os lamellaire en contraste avec la matrice osseuse. E. Microphoto du cortex externe en lumière transmise normale. Le recouvrement plus foncé par le fer préserve les marques de croissance juste au-dessous de la surface corticale, indiquant la fin du second cycle de croissance dans la série de croissance humérale d'*Ophiacodon*. F. Même vue qu'en (E) en lumière transmise polarisée. À noter l'annulus interne du cycle de croissance de la première année. L'annulus corespondant aux marques de croissance en (E) indique aussi le cycle de croissance de la deuxième année. Abréviations : A = annulus ; tri = insertion du muscle triceps.

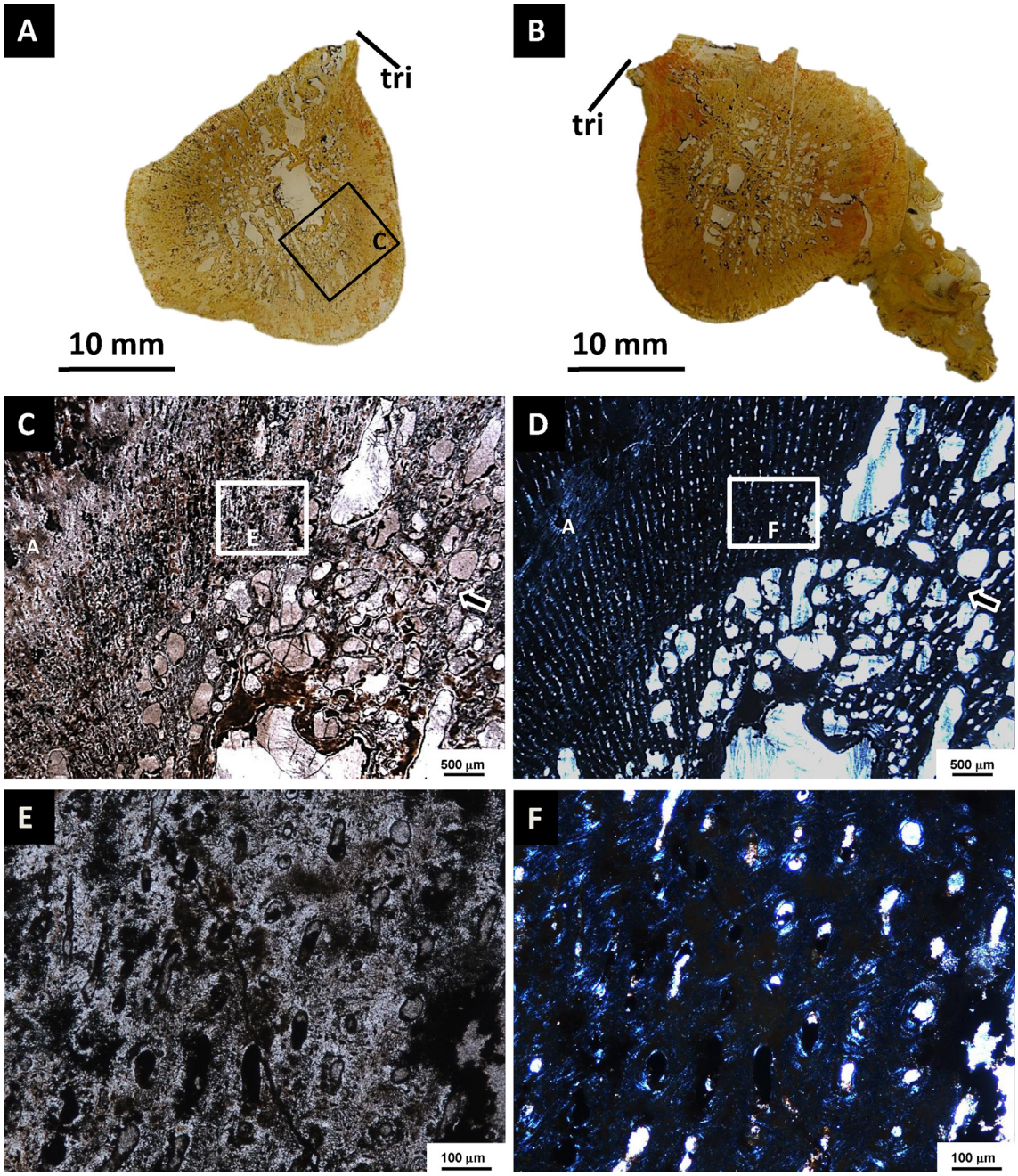

Fig. 8. MCZ-4816, left and right humerus of a MOS IV *O. retroversus* individual. Both of these bones have been affected by recent physical and chemical weathering. A. Scan of the transverse section through the mid-diaphysis of the left humerus. Midshaft is damaged. The cortical bone is thinner and the erosional cavities (EC) are much larger than they were in the previous stage of development, stretching across the cortex. The radial arrangement of vascular canals is seen even in the bone last deposited. B. Scan of the transverse section through the mid-diaphysis of the right humerus. This bone was also incrusted with hematitic or limonitic matrix that incorporated long thin bones from another animal (visible on the lower right). Midshaft is also damaged. C. Photomicrograph of the mid-diaphysis cortex as indicated by the boxed area in (A) in normal transmitted light. The EC appear to be following the pattern of the vascular canals. As the EC develop, they isolate areas of primary cortex that are being incorporated as trabeculae in the medullary cavity and are bounded by lamellar bone (LB). D. Same view as (C) but in polarized transmitted light. The interstitial cortical bone is better visible in polarized light. But because of the poor preservation, the polarized light image gives a false positive for woven (WB) as most of the affected matrix remains dark due to the alteration of the bone apatite crystallites. This has caused areas of parallel-fibered bone (PFB) and most areas of LB to be obscured. Arrow marks the second year cycle boundary that was resistant to resorption. Also, the third year cycle boundary is visible as a thick annulus in the middle cortex marked by "A". E. Magnified view of the cortex indicated by the boxed area (C), in normal transmitted light. The bone matrix is obscured by taphonomic staining rendering proper identification of the specific type of bone matrix difficult; however, it is most likely WB and PFB. F. Same view as in (E) but in polarized transmitted light. Again, most of the LB of the primary osteons lacks birefringence because of poor preservation. Abbreviations: A = annulus; tri = triceps muscle insertion.

smaller and more angular than in MCZ-2819. Primary and, rarely, secondary osteons are observed in the deep cortex (Fig. 9F).

The cortical bone contains a growth record consisting of four zones separated by four LAGs (Table 1), as well as an external fundamental system (EFS) in the outer cortex (Fig. 9B, C, D, E). The EFS itself represents at least eight years of growth and is clearly visible in this specimen (Fig. 9B). Overlapping the growth cycles of this specimen with those of the next smaller, MCZ-4816, and adding the record contained in the EFS, this animal lived at least 16 years (Fig. 5). The reduction of vascularity in the outermost cortex and the presence of the EFS unequivocally indicate that the animal was essentially fully grown or that it had reached the asymptotic phase of growth. The zones in the cortex are heavily vascularized by small longitudinal canals that consist of primary osteons. The zone preceding the EFS has a reduced vascularity and consists of very thin radial canals with almost no LB infilling (Fig. 9D).

As noted, ECs as well as EC lined with lamellar bone persist throughout most of the medullary region, forming trabeculae of interstitial primary cortical bone (Fig. 9F). This trabecular bone occludes the medullary cavity.

4.2.2. *Isolated Ophiacodon uniformis humerus IPBSH-62 (MOS V)*

IPBSH-62 (MOS V; Fig. 4) is a left humerus 82 mm in length (Appendix 1F). The cortex consists of WB and PFB. Vascularity consists of radial and longitudinal canals exhibiting anastomosis (Fig. 10E). Immature and fully formed primary osteons are present in the outer cortex (Fig. 10E and F). Primary osteons and the rarer secondary osteons are observed in the deeper cortex. Interstitial primary cortical bone remains in the medullary margin as secondary trabeculae, similar to what is observed in MCZ-4816 (Fig. 10A and B). Vascularity is more radial in the deeper cortex whereas the vascular canals near the cortical surface are more longitudinal (Fig. 10C). OL are plump to sub-angular in the areas with WB and more flat and oriented parallel to the cortical surface in the areas with PFB. There are very few SFs, and those are only visible under polarized light (Fig. 10F).

Three annuli are visible in the mid to outer cortex (Fig. 10D), the inner two of which contain LAGs (Fig. 10C and D). The earliest LAG is essentially the boundary between the medullary region and the cortex (Fig. 10C and F), as ECs do not extend beyond this area. Also, this LAG is visible in longitudinal section (Fig. 11C and D). This individual died before reaching skeletal maturity because there is no EFS. A thick layer of LB lines the largest ECs in the center of the bone. The histology described here is similar to that described for MCZ-4816 (MOS IV) (Figs. 1 and 4). In the longitudinal section (Fig. 11A and B), it can be seen that the osteocytes in the WB are isometric, indicating that they are indeed static osteocytes while the osteocytes in the PFB are elongate (Fig. 11E and F), indicating that they are spindle-shaped dynamic osteocytes (see Prondvai et al., 2014; Stein and Prondvai, 2014).

4.2.3. *Isolated Ophiacodon sp. humerus OMNH-73698 (MOS IV-V)*

OMNH-73698 (MOS IV-V) is a right humerus 113 mm in length (Appendix 1G) of *Ophiacodon* sp. The histology described here is from a core drilled through the dorsal and ventral sides of the shaft somewhat from the midshaft and closer to the proximal metaphysis (Fig. 12A).

The cortex is thin, presumably because of the location of the sample away from the midshaft. Vascularity appears to be reduced, consisting mainly of small primary osteons and thin radial canals. These are similar to what is seen in the outer cortex of MCZ-1486. The dorsal cortex is mostly PFB with flat OL oriented parallel to the bone surface and reduced vascularity (Fig. 12B). The ventral cortex is WB, and OL are isometric with a dense concentration of SFs (Fig. 12C).

The cortical bone contains an EFS visible in the outermost cortex (Fig. 12B and C); no other growth marks are visible. The medullary cavity consists of secondary trabecular bone with very little interstitial primary cortical bone (Fig. 12A). There are ECs with and without a lining of lamellar bone in the medullary region that extend very close to the outer bone surface (Fig. 12B and C) because of the proximal location of the sample.

4.3. *Ophiacodon femur histology*

The *Ophiacodon* femora (Table 1) are described in order of increasing length (Fig. 2). Overall shape of their cross-sections is affected by the increasing development of the adductor crest with size, but no MOS have been erected for *Ophiacodon* femora.

Fig. 8. Humérus droit et gauche d'un individu *O. retroversus* MCZ-4816, MOS IV. Les deux os ont été affectés par une altération physique et chimique récente. A. Scan de la section transverse à mi-diaphyse de l'humérus gauche. Diaphyse endommagée. L'os cortical est plus mince et les cavités d'érosion (EC) plus grandes qu'ils ne le sont dans le stade précédent de développement, au travers du cortex. L'arrangement radial des canaux vasculaires est observé même dans l'os déposé en dernier. B. Scan de la section transverse à mi-diaphyse de l'humérus droit. Cet os est aussi incrusté d'une matrice hématitique ou limonitique qui a incorporé de longs os minces d'un autre animal (visible en bas à droite de la photo). La diaphyse est également endommagée. C) Microphoto du cortex à mi-diaphyse, comme indiqué par le cadre en AQ) en lumière transmise normale. Les EC suivent le *pattern* des canaux vasculaires. Lorsque les EC se développent, elles isolent des zones de cortex primaire qui sont incorporées sous forme de trabeculae dans la cavité médullaire et sont reliées par de l'os lamellaire. (LB). D. Même vue qu'en (C), mais en lumière transmise polarisée. L'os cortical interstitiel est mieux visible en lumière polarisée. Mais, en raison de la mauvaise conservation, l'image en lumière polarisée donne un faux effet pour l'os tramé (WB), car la plus grande partie de la matrice affectée reste sombre en raison de l'altération des cristallites osseux d'apatite. Ceci induit le fait que l'os à fibres parallèles (PFB) et la plupart des zones de LB sont obscures. La flèche montre la limite avec le cycle de deuxième année qui a résisté à la résorption. La frontière avec le cycle de troisième année est visible sous forme d'un annulus épais marqué « A ». E. Vue agrandie du cortex indiqué par le cadre en (C), en lumière transmise polarisée. La matrice osseuse est obscurcie par la teinture taphonomique, rendant l'identification correcte du type spécifique de matrice osseuse difficile ; cependant, c'est le plus probablement WB et PFB. F. Même vue qu'en (E), mais en lumière transmise polarisée. À nouveau, la plus grande partie de l'os lamellaire (LB) des ostéones primaires manque de biréfringence, en raison d'une mauvaise conservation. Abréviations : A = annulus ; tri = insertion du muscle triceps.

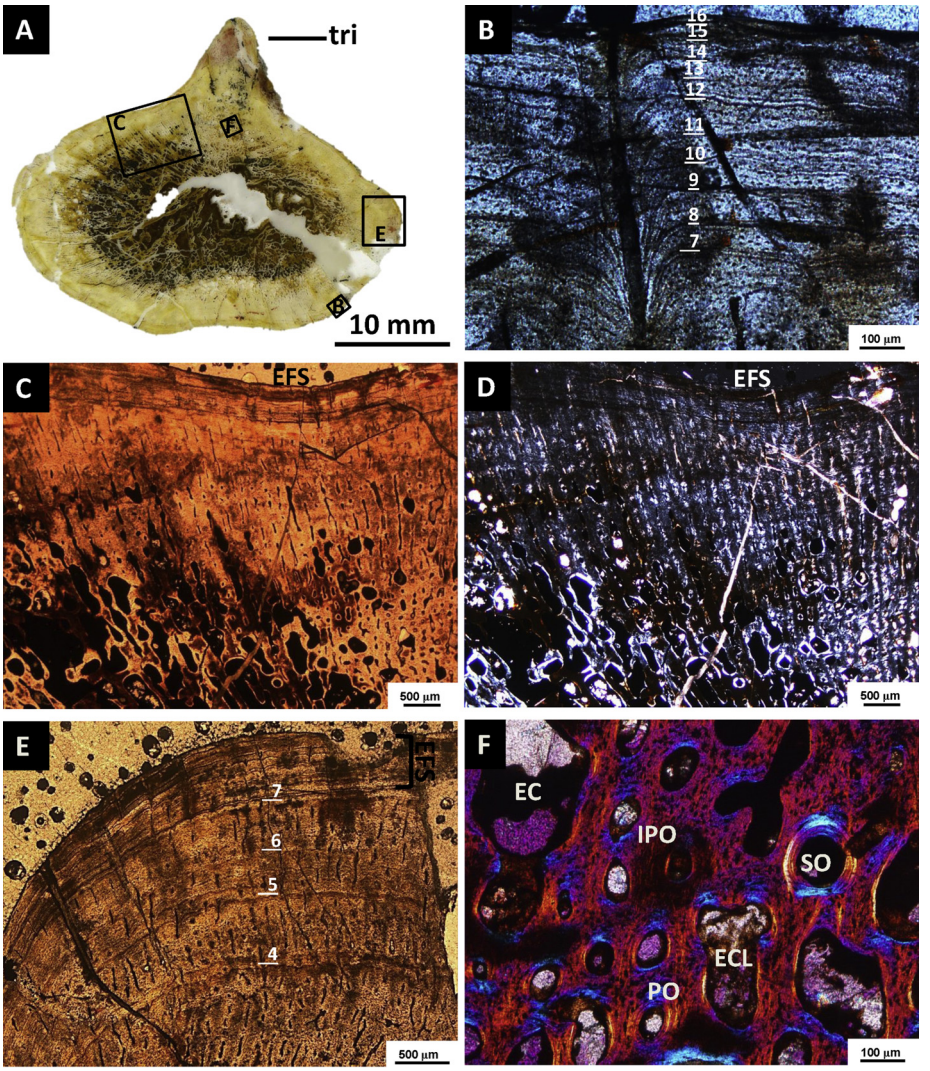

Fig. 9. MCZ-1486, MOS V, *O. retroversus* humerus. A. Scan of the transverse section through the mid-diaphysis. Overall shape of this section is affected by the prominent triceps muscle insertion. Vascularity is highly reduced in the outer cortex but still maintains the "bicycle wheel" pattern of longitudinal and radial canals. B. Photomicrograph of the boxed area in (A) showing the EFS in normal transmitted light with at least eight growth cycles. C. Microscopic view of the mid-diaphysis cortex in normal transmitted light. While retaining a radial orientation, the vascularity diminishes from the medullary cavity to the outer cortex where it is almost nonexistent in the EFS. ECs have not yet reached the outer cortex, but they seem to be following the same pattern, transforming the cortex into cancellous bone with interstitial primary compact bone. D. Same view as (C) in polarized transmitted light. The outwards decreasing vascularity is better observed in this light. ECs are lined by a thin layer of LB. E. Photomicrograph of the outer cortex as indicated by the boxed area in (A) in normal transmitted light. The growth record preserved here consists of four cycles ending in LAGs, representing years 4 to 7. Note that most of the LAGs are double. Skeletal maturity was reached after the seventh life cycle. F. Photomicrograph of boxed area indicated in (A) in polarized transmitted light with lambda filter. This area is just beneath the triceps muscle insertion. Primary woven cortex is prevalent, and OL are isometric and numerous. Abbreviations: EC = erosional cavity; EFS = external fundamental system; IPO = incipient primary osteons; PO = primary osteons; ECL = erosional cavity with a thin lining of lamellar bone; SO = secondary osteon; tri = triceps muscle insertion.

Fig. 9. Humérus MCZ-1486, MOS V d'*O. retroversus*. A. Scan de la section transverse à mi-diaphyse. La forme d'ensemble de la section est affectée par l'insertion saillante du triceps. La vascularisation est très réduite dans le cortex externe, mais elle garde le *pattern* « en roue de bicyclette » des canaux longitudinaux et radiaux. B. Microphoto de la zone encadrée en (A) montrant les EFS en lumière transmise normale avec au moins huit cycles de croissance. C. Microphoto du cortex à mi-diaphyse, en lumière transmise normale. Tandis qu'une orientation radiale est maintenue, la vascularisation diminue de la cavité médullaire jusqu'au cortex externe, où elle est presque inexistante dans les EFS. Les cavités d'érosion n'ont pas encore atteint le cortex externe, mais elles semblent suivre le même *pattern* transformant le cortex en os oblitéré par de l'os compact primaire interstitiel. D. Même vue qu'en (C), en lumière transmise polarisée. La vascularisation décroissante à l'extérieur est plus facile à observer à cette lumière. Les cavités d'érosion sont bordées par un mince feuillet de LB. E. Microphoto du cortex externe tel qu'indiqué dans la zone encadrée en (A), en lumière transmise normale. L'enregistrement de la croissance préservée ici fait état de quatre cycles se terminant en LAGs, représentant les années 4 à 7. À noter que la plupart des LAGs sont doubles. La maturité du squelette a été atteinte après le septième cycle de vie. F. Microphoto de la zone encadrée en (A), en lumière transmise polarisée, avec filtre lambda. Cette zone est juste en dessous de l'insertion du muscle triceps. Le cortex tramé primaire est prédominant et les OL sont isométriques et en nombre. Abréviations : EC = cavité d'érosion, EFS = système fondamental externe ; IPO = ostéones primaires naissantes ; PO = ostéones primaires ; ECL = cavité d'érosion avec une fine bordure d'os lamellaire ; SO = ostéone secondaire ; tri = insertion du muscle triceps.

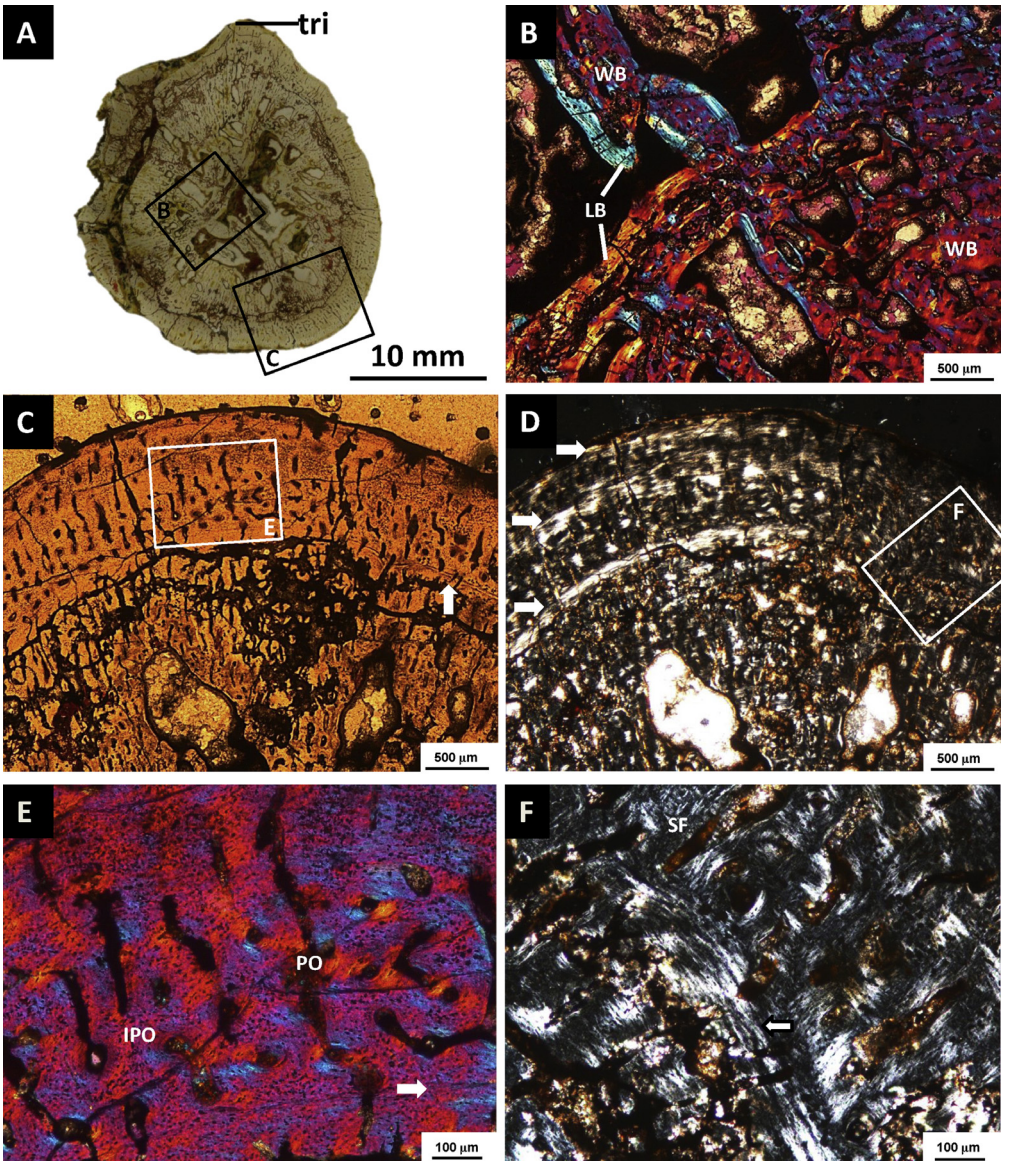

Fig. 10. IPBSH-62 MOS V, *O. uniformis* humerus. A. Scan of the transverse section through the mid-diaphysis. The triceps muscle insertion is much smaller than what is seen in *O. retroversus* at MOS V. Erosional cavities are in the mid to lower cortex but do not yet cross the innermost LAG. Histology is similar to what was described in MCZ-4816. Note the lack of an external fundamental system. B. Photomicrograph of boxed area indicated in (A) viewed in polarized light and a lambda filter. Large areas of interstitial primary cortex of woven bone (WB) are incorporated into secondary trabecular bone. Primary osteons are present here in the oldest areas of the cortex. C. View of the boxed area in (A) in normal transmitted light. The "bicycle wheel" pattern is present in the cortex, consisting of radial and longitudinal canals with a varying degree of anastomosis. Arrow is pointing to the LAG. D. Same view as (C) in polarized light. Arrows indicate annuli. E. Photomicrograph of boxed area indicated in (C) viewed in polarized light and a lambda filter. Note the combination of both incipient and primary osteons. Arrow points to the LAG. F. Photomicrograph of boxed area in (D) in polarized transmitted light. Arrows indicates Sharpey's fibers and the LAG. Overall the cortical matrix consists of WB. Abbreviations: A = annulus; IPO = incipient primary osteon; PO = primary osteon; SF = Sharpey's fibers; tri = triceps muscle insertion; Z = zone.

Fig. 10. Humérus IPBSH-62, MOS V d'*O. uniformis*. A. Scan de la section transverse à mi-diaphyse. L'insertion du muscle triceps est beaucoup plus petite que ce qui est observé chez *O. retroversus* à MOS V. Les cavités d'érosion se développent du cortex moyen à inférieur, mais n'ont pas encore traversé la LAG la plus interne. L'histologie est similaire à celle qui a été observée en MCZ-4816. À noter le manque de système fondamental externe. B. Microphoto de la zone encadrée en (A), en lumière polarisée avec filtre lambda. De grandes zones de cortex interstitiel d'os tramé (WB) sont incorporées dans de l'os trabéculaire secondaire. Les ostéones primaires sont ici présentes dans les zones anciennes du cortex. C. Vue de la zone encadrée en (A), en lumière transmise normale. Le *pattern* en « roue de bicyclette » est présent dans le cortex, consistant en canaux longitudinaux et radiaux, avec un degré variable d'anastomose. La flèche pointe sur la LAG. D. Même vue que (C), en lumière polarisée. Les flèches indiquent les annuli. E. Microphoto de la zone encadrée en (C) vue en lumière polarisée avec un filtre lambda. À noter la combinaison entre ostéones naissantes et primaires. La flèche pointe sur la LAG. F. Microphoto de la zone encadrée en (D) en lumière transmise polarisée. La flèche indique les fibres de Sharpey et la LAG. La matrice corticale d'ensemble est constituée de WB. Abréviations : A = annulus ; IPO = ostéone primaire naissante ; PO = ostéone primaire ; SF = fibres de Sharpey ; tri = insertion du muscle triceps ; Z = zone.

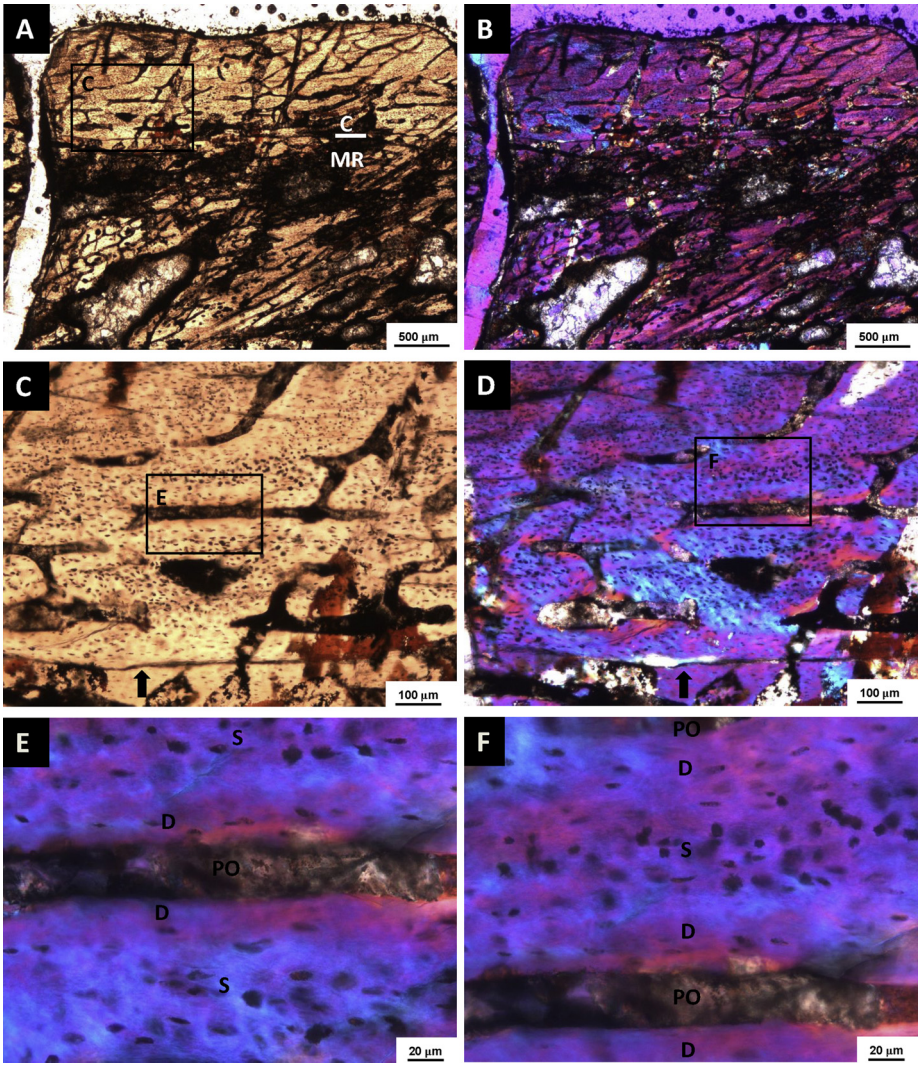

Fig. 11. IPBSH-62, MOS V, *O. uniformis* humerus. A. Photomicrograph of a longitudinal section of the mid-diaphysis in normal transmitted light. The outer bone surface is at the top of the image. Compare this figure to Fig. 10C which shows the same region of the cortex in transverse section. Longitudinal canals have been bisected and are running parallel and perpendicular to the bone surface. The medullary region is marked by erosional cavities. B. Same view as in (A) viewed in polarized light with a lambda filter. Note the primary osteons. C. Photomicrograph of boxed area in (A) viewed in normal transmitted light. Arrow is pointing to the line of arrested growth (LAG) that was visible in the transverse section as a double LAG. This growth mark essentially is the border between the lower cortex and the medullary region. D. Same view as in (C) imaged in polarized light with a lambda filter. Note that the region with the static osteocytes shows magenta colors, suggesting random bone crystallite orientation, as opposed to the region with dynamic osteocytes. E. Photomicrograph of boxed area in (C) imaged in polarized light with a lambda filter. Note the presence of both static and dynamic osteocytes. Dynamic osteocytes are embedded in parallel-fibered bone (PFB) matrix surrounding the vascular canals, forming a primary osteon. Static osteocytes are embedded in the interstitial woven bone matrix. F. Photomicrograph of boxed area in (D) in polarized light with a lambda filter. Note the interstitial woven matrix indicated by the static osteocytes. PFB matrix containing dynamic osteocytes surrounds the vascular canals, thus forming primary osteons. Abbreviations: C = cortex; D = dynamic osteocytes; MR = medullary region; PO = vascular canal in center of primary osteon; S = static osteocytes.

Fig. 11. Humérus IPBSH-62, MOS V d'*O. uniformis*. A. Microphoto d'une section longitudinale à mi-diaphyse, en lumière transmise normale. La surface osseuse externe est au sommet de l'image. Cette figure est à comparer à la Fig. 10C qui montre la même zone de cortex en coupe transverse. Les canaux longitudinaux ont été divisés en deux et courent parallèlement et perpendiculairement à la surface osseuse. La zone médullaire est marquée par des cavités d'érosion. B. Même vue qu'en (A), en lumière polarisée avec un filtre lambda. À noter les ostéones primaires. C. Microphoto de la zone encadrée en (A), en lumière transmise normale. La flèche pointe sur la ligne d'arrêt de croissance (LAG) qui est visible en section transverse sous forme d'une LAG double. D. Même vue qu'en (C) en lumière polarisée avec un filtre lambda. À noter que la zone à ostéocytes statiques montre des couleurs magenta, suggérant une orientation aléatoire des cristallites osseux, opposée à la zone à ostéocytes dynamiques. E. Microphoto de la zone encadrée en (C), en lumière polarisée avec un filtre lambda. À noter la présence d'ostéocytes à la fois statiques et dynamiques. Les ostéocytes dynamiques sont inclus dans une matrice osseuse à fibres parallèles (PFB) environnant les canaux vasculaires formant une ostéone primaire. Les ostéocytes statiques sont inclus dans la matrice osseuse interstitielle tramée. F. Microphoto de la zone encadrée en (D) en lumière polarisée avec un filtre lambda. À noter la matrice interstitielle tramée indiquée par les ostéocytes statiques. La matrice PFB contenant les ostéocytes dynamiques entoure les canaux vasculaires, formant ainsi les ostéones primaires. Abréviations : C = cortex ; D = ostéocytes dynamiques ; MR = zone médullaire ; PO = canal vasculaire au centre d'une ostéone primaire ; S = ostéocytes statiques.

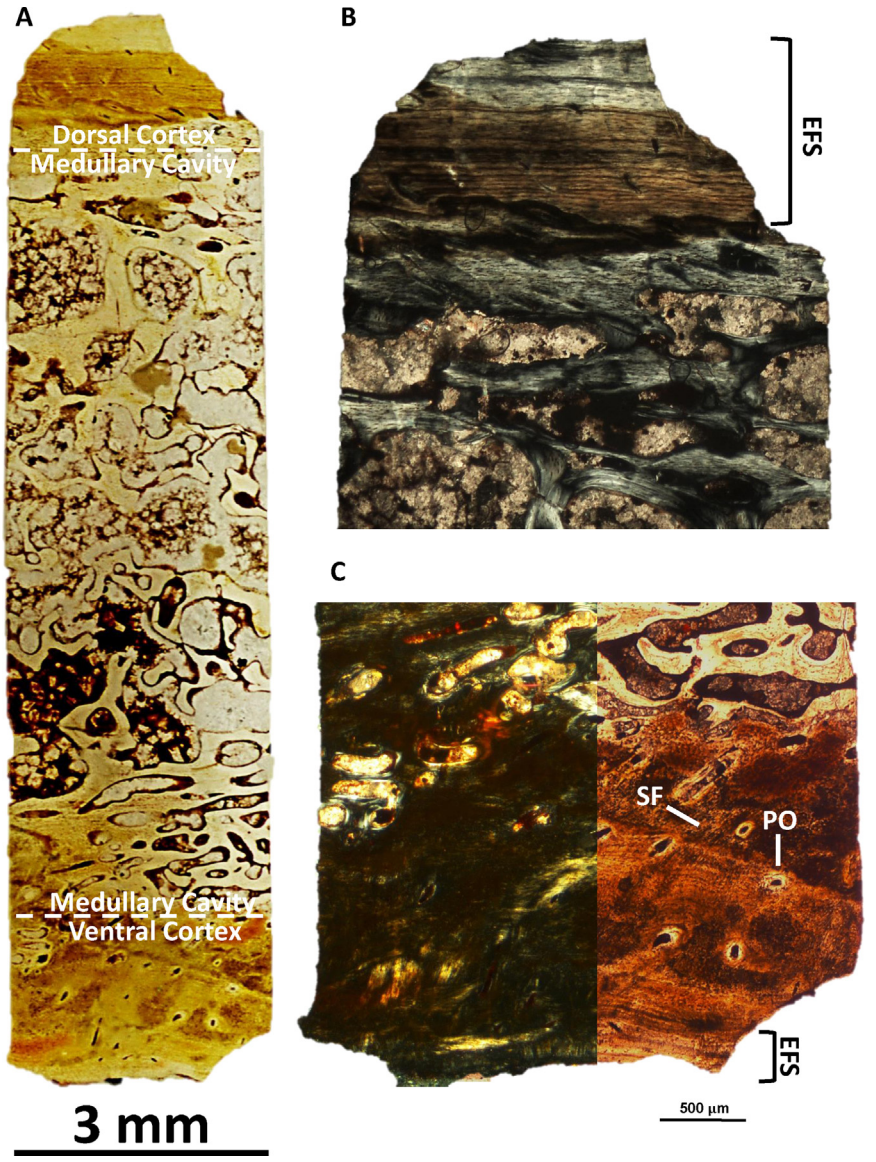

Fig. 12. OMNH-73698, MOS IV-V, *Ophiacodon* sp. humerus. A. Scan of a transverse core section drilled through the dorsal and ventral sides of the diaphysis close to the proximal metaphysis. The cortex is thin and vascularity is highly reduced in the dorsal cortex. The ventral cortex contains small primary osteons and larger incipient osteons. Notice the EFS and that the vascular canals are smaller on the dorsal side and near the EFS. The medullary cavity is occluded by secondary trabeculae. B. Photomicrograph of the EFS in the dorsal cortex in polarized transmitted light. The cortical bone matrix of the dorsal side is mostly parallel-fibered bone with a strong lamellar bone affinity. C. Magnified view of the ventral cortex in normal transmitted light. This area is highly concentrated with Sharpey's fibers. Osteocyte lacunae are rounder and randomly oriented. The cortical bone matrix below the EFS on the ventral side is woven bone. Abbreviations: EFS = external fundamental system; PO = primary osteon.

Fig. 12. Humérus OMNH-73698, MOS IV-V d'*Ophiacodon* sp. A. Scan d'une section transverse de carotte prélevée au travers des parties dorsale et ventrale de la diaphyse près de la métaphyse proximale. Le cortex est mince et la vascularisation nettement réduite dans le cortex dorsal. Le cortex ventral contient de petites ostéones primaires et de grandes ostéones naissantes. À noter l'EFS et le fait que les canaux vasculaires sont plus petits sur le côté dorsal et près de l'EFS. La cavité médullaire est occluse par des trabeculae secondaires. B. Microphoto de l'EPS dans le cortex dorsal en lumière transmise polarisée. La matrice osseuse corticale du côté dorsal est en grande partie constituée d'os à fibres parallèles, à grande affinité osseuse lamellaire. C. Vue agrandie du cortex ventral en lumière transmise normale. Cette zone est très concentrée en fibres de Sharpey. Les lacunes d'ostéocytes sont plus rondes et orientées de manière aléatoire. La matrice osseuse corticale au-dessous de l'EPS sur le côté ventral est faite d'os tramé. Abréviations : EFS = système fondamental externe ; PO = ostéone primaire.

4.3.1. Isolated Ophiacodon sp. femur IPBSH-46

IPBSH-46 is a right femur 78 mm in length (Appendix 2A). This specimen is the smallest femur sampled. The outer surface is smooth, and the epiphyses are poorly ossified. The bone is dorsoventrally crushed along the diaphysis (Fig. 13A) and distal end. Histology is similar to what is seen in humerus MCZ-5926 (MOS II) including extensive preservation of embryonic bone inside the HL. The embryonic bone is mostly WB with large wide radial and longitudinal vascular canals (Fig. 13B and E). The onset

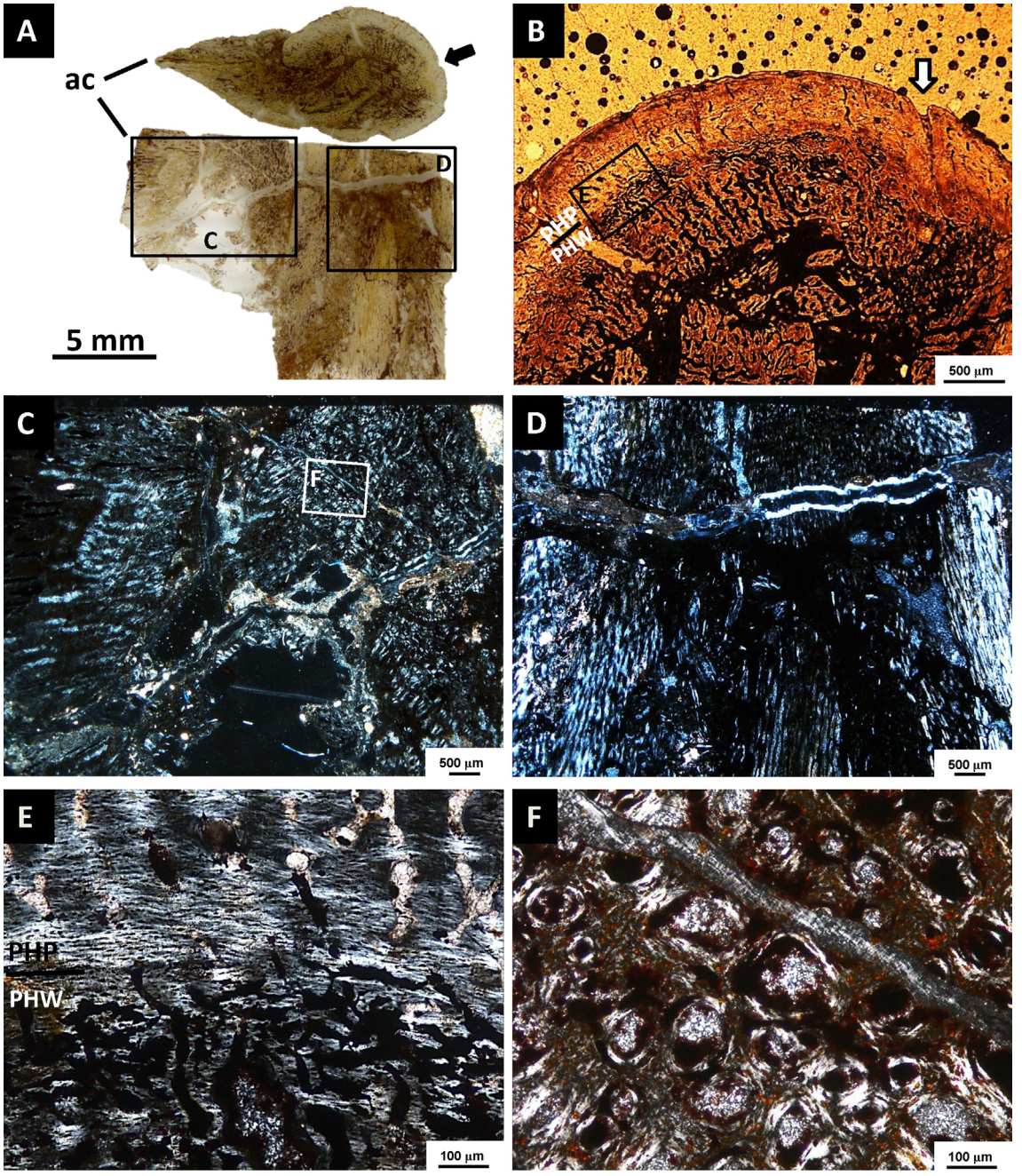

Fig. 13. IPBSH-46, *Ophiacodon* sp. femur, 78 mm in length. A. Scan of the transverse (above) and longitudinal section (below) of the mid-diaphysis. Even though the midshaft is crushed, there is a marked distinction between the pre-hatching and post-hatching cortex, separated by the hatching line (HL). Arrow indicates the nutrient canal on the dorsal side. B. Photomicrograph of the dorsal cortex in normal transmitted light. Arrow indicates the nutrient canal that extends into the pre-hatching cortex. Vascular canals in the pre-hatching bone are larger than those in the post-hatching bone. Vascularity consists of longitudinal, radial and reticular canals. Vascularity in the deep pre-hatching cortex somewhat resembles the "bicycle wheel" pattern seen in the humeri. However, this is not the case in the post-hatching cortex as the vascularity is more reticular. This animal was within the first year of its life when it died. C. Photomicrograph of boxed area in (A) of the longitudinally sectioned adductor crest in polarized transmitted light. Note the high concentrations of primary osteons in the woven bone (WB) matrix. D. Photomicrograph of boxed area in (A) of the longitudinally sectioned diaphysis in polarized transmitted light. Note the extreme vascularity throughout the bone tissue. E. Photomicrograph of boxed area in (B) in polarized transmitted light. Most striking is the sudden change from the pre-hatching woven bone in the inner cortex and the post-hatching parallel-fibered bone in the mid- to outer cortex at the HL. Incipient primary osteons are prevalent in the outer cortex. Note the high vascularity in the pre-hatching bone. F. Photomicrograph of the boxed area in (C) in polarized transmitted light. Note the large primary osteons and isometric osteocyte lacunae set within a WB matrix. This tissue is characteristic of fetal fibrolamellar bone. Abbreviations: ac = adductor crest; PHP = post-hatching parallel-fibered bone; PHW = pre-hatching woven bone.

of PFB in the mid-cortex is marked by the distinctive HL (Fig. 13B and E). The circumference of the HL cannot be measured exactly because of crushing but seems to have been greater than in the small *O. retroversus* humerus MCZ-5926. The nutrient canal is located in the dorsal region (Fig. 13A) of the shaft cross-section. It extends from the pre-hatching cortex and the MC to the outermost cortical layer (Fig. 13B). The periosteal bone is well vascularized in the outer cortex by longitudinal and reticular canals. The posterior region, where the adductor crest is located, consists mostly of radial canals (Fig. 13A and C). The vascular pattern is longitudinal and reticular in the post-hatching area, but the vascularity of the pre-hatching area is more radial (Fig. 13E).

The vascular canals themselves have varying degrees of LB infilling in that most represent incipient primary osteons in the post-hatching cortex, but there are many fully formed primary osteons in the pre-hatching areas (Fig. 13C and F). OL shape in pre-hatching WB are isometric while those in the post-hatching PFB are more flattened and oriented parallel to the cortical surface. The tissue in the deep cortex thus is best called embryonic fibrolamellar bone.

The growth record contained in the cortex indicates that the individual most likely died within the first year of its life, shortly after hatching (Fig. 13B). The MC is obscured due to deformation; trabecular bone is not evident, but a few small ECs appear around the medullary cavity (Fig. 13A and B).

4.3.2. *Isolated Ophiacodon mirus femur OMNH-55234*

OMNH-55234 is an incomplete right femur (100 mm in length) (Appendix 2B). The adductor crest is damaged (Fig. 14A). The cortical bone consists of WB and PFB alternating as zones and annuli (Fig. 14D). The vascularity is radially arranged, similar to what is observed in the humeri, forming an overall "bicycle wheel" pattern in the deep cortex (Fig. 14C and D). Vascularity remains radial until it reaches the first LAG and then it changes to a more reticular pattern (Fig. 14B). Primary osteons are present throughout the cortex (Fig. 14E and F). OL are isometric and plump in the zones and more flattened in the annuli (Fig. 14E).

The cortex contains a growth record of three zones separated by two LAGs set in annuli (Fig. 14C and D), suggesting that the animal died in its third year of life. It is worth noting that the amount of WB decreases from the inner to the outer cortex (Fig. 14D). Also, in the dorsal region of the outer cortex, perpendicular to the bone surface, the lining of the nutrient canal extends deep into the medullary region (Fig. 14B).

The medullary region is occluded by secondary trabeculae and bound by large ECs in the process of complete resorption of the primary cortex and formation of secondary trabecular bone (Fig. 14A). A few ECs have appeared in the deep cortex. Endosteal resorption/redeposition is strongest in the posterior region. A free medullary cavity is present, unlike what is observed in any of the sampled humeri.

4.3.3. *Isolated Ophiacodon uniformis femur MSU uncatalogued*

The MSU specimen is a left femur, 115 mm in length (Appendix 2C) with a damaged adductor crest (Fig. 15A). In the transverse section, it can be seen that the cortical bone consists of WB and PFB alternating as zones and annuli (Fig. 15D). The vascularization is reticular and longitudinal with sparse thin radial canals (Fig. 15C and D). OL range in shape from isometric to linear (Fig. 15B). Incipient and fully formed primary osteons are visible throughout the cortex, but secondary osteons are concentrated near the borders of the medullary region (Fig. 15E and F).

An extensive growth record is contained in the periosteal bone. At least eight growth cycle boundaries are marked by annuli four of which correspond with LAGs (Fig. 15C and D). The cortex contains one large annulus at the medullary boundary, but it is in the process of being resorbed. This could be the first complete cycle of growth; although earlier growth marks could have been lost to resorption. ECs have already formed and extended to the fifth annulus. The nutrient canal in the dorsal region of the outer cortex is similar to those in OMNH-55234 and IPBSH-46 (Fig. 15A, C, D).

The medullary margin is bound by many ECs with and without a lining of lamellar bone that extend to the mid-cortex. The MC is occluded by trabecular bone (Fig. 15A).

4.3.4. *Isolated Ophiacodon retroversus femur OMNH-35389*

OMNH-35389 is a left femur with an overall length of 221 mm (Appendix 2D); this is the largest femur sampled. The histology described here is from a core drilled in the dorsal side of the midshaft. The cortical bone consists of

Fig. 13. Fémur IPBSH-46 d'*Ophiacodon* sp., longueur 78 mm. A. Scan de section transverse (en haut) et longitudinale (en bas) à mi-diaphyse. Bien que la diaphyse soit broyée, il y a une distinction marquée entre les cortex pré-éclosion et post-éclosion, séparés par la ligne d'éclosion (HL). La flèche indique le canal nourricier sur le côté dorsal. B. Microphoto du cortex dorsal en lumière transmise normale. La flèche indique le canal nourricier qui se développe à l'intérieur du cortex pré-éclosion. Les canaux vasculaires dans l'os pré-éclosion sont plus larges que dans la zone post-éclosion. La vascularisation consiste en canaux longitudinaux, radiaux et réticulés. La vascularisation dans la partie profonde du cortex pré-éclosion ressemble quelque peu au *pattern* « en roue de bicyclette » observé dans les humérus. Cependant, ce n'est pas le cas dans le cortex post-éclosion, car la vascularisation est plus réticulaire. Cet animal était dans la première année de sa vie, lorsqu'il est mort. C. Microphoto de la zone encadrée en (A) de la crête adductrice sectionnée longitudinalement, en lumière transmise polarisée. À noter la forte concentration d'ostéones primaires dans la matrice osseuse tramée (WB). D. Microphoto de la zone encadrée en (A) de la diaphyse sectionnée longitudinalement, en lumière transmise polarisée. À noter la vascularisation extrême au travers du tissu osseux. E. Microphoto de la zone encadrée en (B), en lumière transmise polarisée. Le plus surprenant est le changement soudain à partir de l'os tramé pré-éclosion dans le cortex interne et l'os post-éclosion à fibres parallèles dans le cortex moyen et externe. Les ostéones primaires naissantes sont prédominantes dans le cortex externe. À noter la vascularisation importante dans l'os pré-éclosion. F. Microphoto de la zone encadrée en (C), en lumière transmise polarisée. À noter les grandes ostéones primaires et les lacunes d'ostéocytes isométriques au sein de la matrice WB. Ce tissu est caractéristique de l'os fibro-lamellaire fœtal. Abréviations : ac = crête adductrice ; PHP = os post-éclosion à fibres parallèles ; PHW = os tramé pré-éclosion.

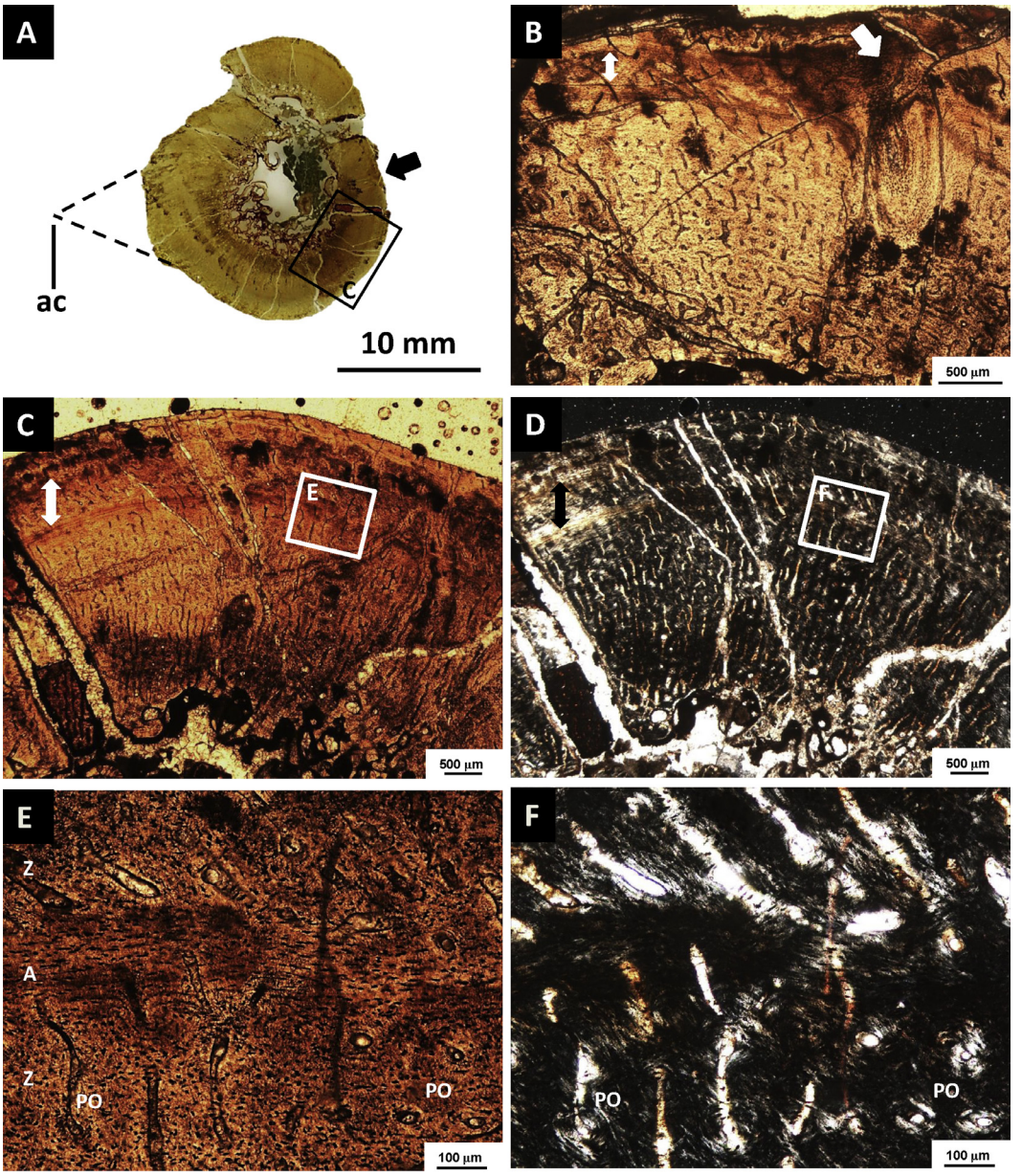

Fig. 14. OMNH-55234 *O. mirus* femur 100 mm in length. A. Transverse section through the mid-diaphysis. The midshaft is damaged and the adductor crest is incomplete (reconstruction of the missing area is general and not an accurate morphological reconstruction). Arrow is pointing to the location of the nutrient canal. B. Photomicrograph of the dorsal cortex in normal transmitted light. Arrow is pointing to lining of the nutrient canal. Surrounding vascularity is reticular. C. Microscopic view of the mid-diaphysis cortex in normal transmitted light of the boxed area in (A). Double-headed arrow is pointing to the lines of arrested growth (LAGs). D. Same view as in (C) but in polarized transmitted light. Note the radial and longitudinal canals form the same "bicycle wheel" pattern as that seen in the humeri below the inner LAG. Small reticular vascular canals are also present above this LAG. E. Photomicrograph of the boxed area in (C) in normal transmitted light. Osteocyte lacunae appear flat and generally oriented parallel to the cortical surface within the annulus. F. Same view as in (E) in polarized transmitted light. Note the primary osteons set in a woven bone matrix, i.e., fibrolamellar bone. Abbreviation: ac = adductor crest.

Fig. 14. Fémur OMNH-66234 d'*O. mirus*, longueur 10 mm. A. Section transverse à mi-diaphyse. La diaphyse est endommagée et la crête adductrice est incomplète (la reconstitution de la zone manquante est générale et ce n'est pas une reconstitution morphologique précise). La flèche pointe sur la localisation du canal nourricier. B. Microphoto du cortex dorsal, en lumière transmise normale. La flèche pointe sur la bordure du canal nourricier. La vascularisation à l'entour est réticulée. C. Vue microscopique du cortex à mi-diaphyse, en lumière transmise normale dans la zone encadrée en (A). La flèche à deux pointes indique les lignes de croissance arrêtée (LAGs). D. Même vue qu'en (C), mais en lumière transmise polarisée. À noter que les canaux longitudinaux et radiaux forment le même *pattern* « en roue de bicyclette » que celui observé dans les humérus, au-dessous de la LAG interne. De petits canaux vasculaires réticulés sont aussi présents au-dessus de cette LAG. E. Microphoto de la zone encadrée en (C), en lumière transmise normale. Les lacunes d'ostéocytes apparaissent aplaties et orientées parallèlement à la surface corticale au sein de l'annulus. F. Même vue qu'en (E) en lumière transmise polarisée. À noter les ostéones primaires dans une matrice osseuse tramée, c'est-à-dire d'os fibro-lamellaire. Abréviation : ac = crête adductrice.

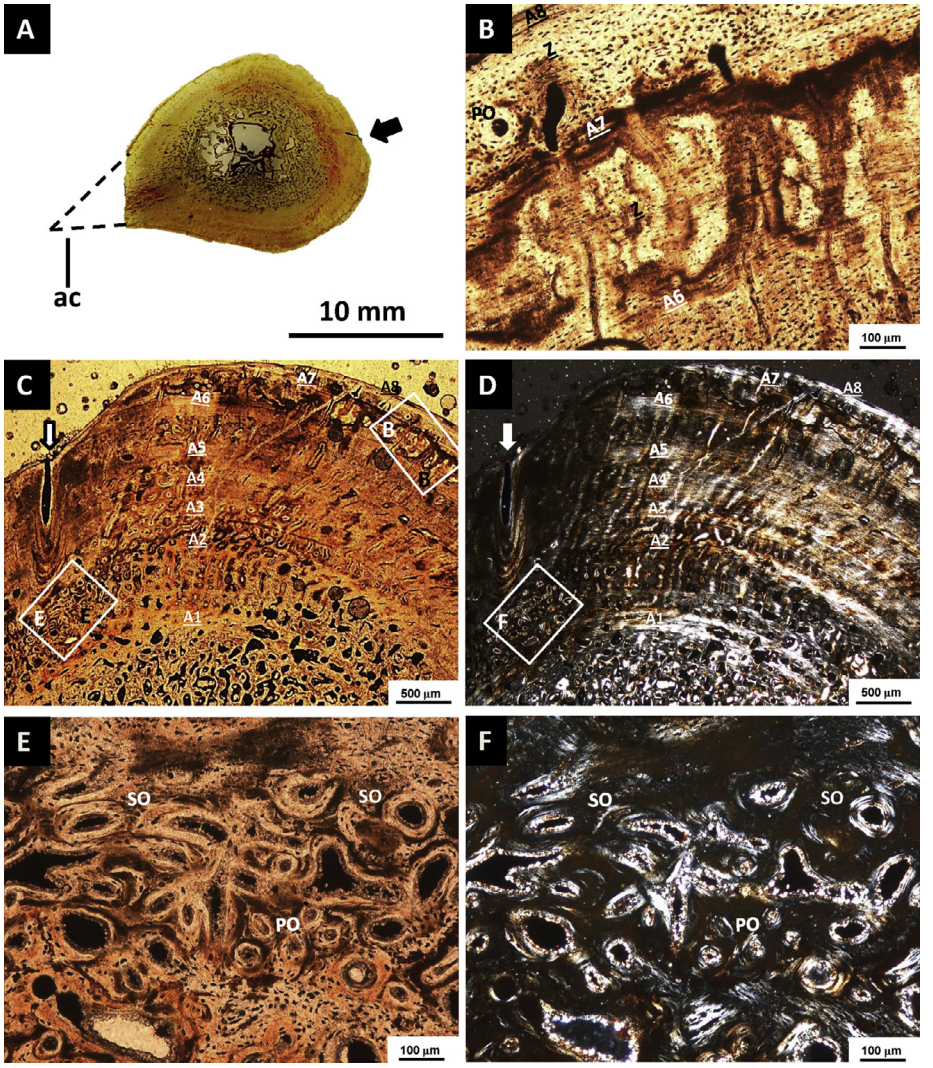

Fig. 15. Uncatalogued MSU femur, *O. uniformis*, 115 mm in length. A. Scan of the transverse section of the mid-diaphysis. The midshaft is damaged and the adductor crest is incomplete (reconstruction of the missing area is general and not an accurate morphological reconstruction). Arrow indicates the nutrient canal. B. Photomicrograph of the boxed area in (C) in normal transmitted light. Alternating zones and annuli can be observed. C. Magnified view of the dorsal cortex in normal transmitted light. Arrow indicates the nutrient canal that extends into the deep cortex. Note how the cortex was affected during ontogeny to continually incorporate this permanent structure throughout the life of the animal. The cortical growth record consists of eight annuli (parallel-fibered bone), some of which are associated with lines of arrested growth. The oldest annulus (A1) is the boundary between the cortex and the medullary region. The inner cortical vascularity is longitudinal. The mid-cortex is a combination of longitudinal and reticular canals. In the outermost cortex, there are thin zones (woven bone) with one to two rows of longitudinal primary osteons. Secondary trabeculae occlude the medullary cavity. D. Same view as in (C) but in polarized transmitted light. Annuli are better visible in polarized light. Notice that the vascularization does not form the same "bicycle wheel"pattern as that seen in OMNH-55234. E. Photomicrograph of the boxed area in (C) in normal transmitted light just below the nutrient canal. Note the combination of primary and secondary osteons. F. Same view as in (E) in polarized transmitted light. Abbreviations: A = annulus; ac = adductor crest; PO = primary osteon; SO = secondary osteon; Z = zone.

Fig. 15. Fémur MSU, non catalogué d'*O. uniformis*, longueur 115 mm. A. Scan de la section transverse à mi-diaphyse. La diaphyse est endommagée et la crête adductrice est incomplète (la reconstitution de la zone manquante est générale, et ce n'est pas une reconstitution morphologique précise). La flèche indique le canal nourricier. B. Microphoto de la zone encadrée en (C) en lumière transmise normale. On peut observer l'alternance de zones et d'annuli. C. Vue agrandie du cortex dorsal, en lumière transmise normale. La flèche indique le canal nourricier qui se développe dans la partie profonde du cortex. À noter comment, au cours de l'ontogénie, le cortex a été affecté, pour incorporer continuellement cette structure permanente tout au long de la vie de l'animal. Le relevé de la croissance corticale indique huit annuli (os à fibres parallèles), dont certains sont associés aux lignes de croissance arrêtée. Le plus ancien annulus (A1) est à la frontière entre le cortex et la zone médullaire. La vascularisation corticale interne est longitudinale. Le cortex médian consiste en une combinaison de canaux longitudinaux et réticulés. Dans le cortex externe, il y a des zones minces (os tramé), avec une ou deux rangées d'ostéones primaires longitudinales. Des trabeculae secondaires ferment la cavité médullaire. D. Même vue qu'en (C), mais en lumière transmise polarisée. Les annuli sont plus visibles en lumière polarisée. À noter que la vascularisation ne forme pas le même *pattern* « en roue de bicyclette » que celui observé en OMNH-55234. E. Microphoto de la zone encadrée en (C), en lumière transmise normale, juste au-dessous du canal nourricier. À noter la combinaison ostéones primaires et secondaires. F. Même vue qu'en (E), en lumière transmise polarisée. Abréviations : A = annulus ; ac = crête adductrice ; PO = ostéone primaire ; SO = ostéone secondaire ; Z = zone.

WB and PFB with alternating zones and annuli (Fig. 16A and B). Vascularization is mainly restricted to the zones and is found in reticular, radial, and longitudinal patterns, decreasing in density from the deep inner cortex to the outer cortex (Fig. 16C). Vascular canals are more radial in the deeper primary cortex and become more reticular towards the outer surface (Fig. 16A). OL are plump in the deep cortex and in the zones, but they are flat in the annuli and EFS (Fig. 16C). Primary osteons are mostly incipient in the outer cortex, but fully formed osteons are observed in the deeper cortex.

The cortical bone contains eight growth cycles ending in annuli (Fig. 16A) and one very prominent LAG marking the start of the EFS in the outermost cortex (Fig. 16C). Any growth cycles earlier than the one ending in the innermost annulus have been resorbed (Fig. 16B). This is the only femur to exhibit an EFS; however, the exact number of growth cycles in the EFS remains unknown due to the diagenetic staining (Fig. 16C). The EFS indicates that the animal had reached skeletal maturity. The medullary cavity appears to be open with extensive ECs extending to the base of the third growth cycle. Secondary trabeculae are present. There is much more endosteal resorption and redeposition of cortical bone in contrast to what was observed in the humeri.

4.4. Ontogenetic age and skeletochronological data

Growth mark count and age estimate for each of the four *O. retroversus* humeri studied by Brinkman (1988) are provided in Table 1. The first fully completed growth cycle is still visible in the smallest humerus sampled (MCZ-5926; MOS II) (Fig. 6C). This cycle is the area between the HL and the first growth mark in the outermost cortex. By using a method similar to that of Bybee et al. (2006), we estimate that this growth series represents seven years of growth between the time of hatching and the year skeletal maturity was achieved. At least another eight cycles were visible in the external fundamental system (EFS) of MCZ-1486 (see Fig. 9B). Assuming the cycles in the EFS to be annual, this means that the largest *Ophiacodon* in our sample grew substantially for half of its life. The estimated total lifespan represented by this growth series thus is at least 16 years (Fig. 5). However, we cannot assume that we sampled the oldest individuals in the population. Our analysis revealed a discrepancy between MCZ-4816 (MOS IV) and MCZ-1486 (MOS V) because of the uncertain matching of the absent fourth cycle in MCZ-4816, and the third cycle boundary in MCZ-1486, which is assumed to have been resorbed. This results in a margin of error of at least one year. The time represented by Brinkman's (1988) *O. retroversus* humeral growth series (Fig. 1) is consistent with the growth record preserved in some of our *Ophiacodon* femora (MSU uncatalogued and OMNH-35389) (see Figs. 15 and 16).

5. Discussion

In this study, we focused on the long bone histology of the basal synapsid *Ophiacodon* from Texas and Oklahoma localities of various geological ages in order to investigate what previous studies called "fast growing" tissue as

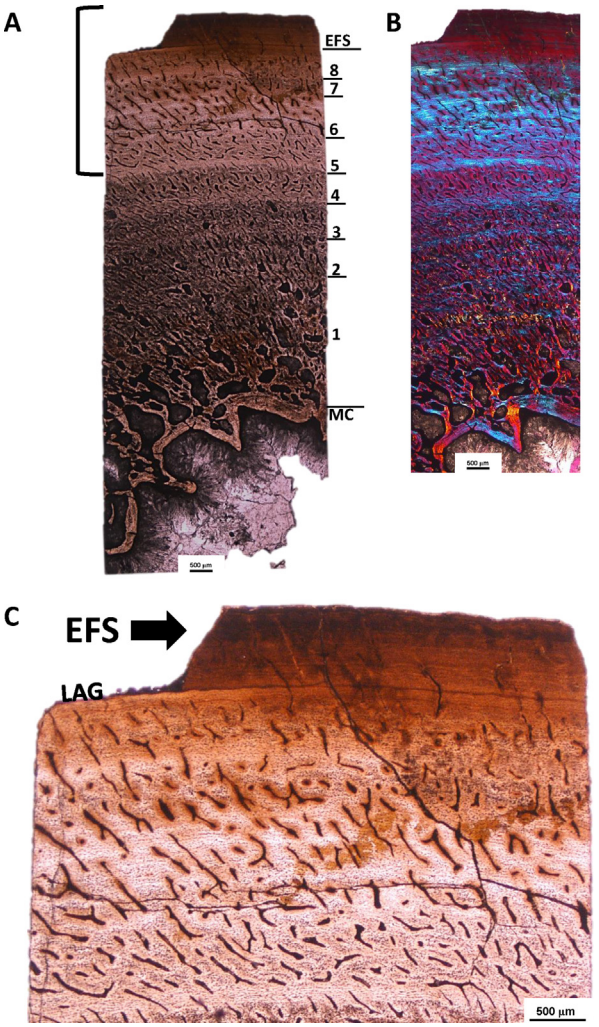

Fig. 16. OMNH-35389 *O. retroversus* femur 221 mm in length. A. Scan of a transverse core section drilled into the dorsal sides of the mid-diaphysis. A distinctive EFS can be seen in the outer cortex. Vascularity consists of longitudinal and reticular canals. In addition to the EFS, eight growth cycles can be seen in the cortex. Earlier growth cycles may have been resorbed. Erosional cavities do not extend beyond the third cycle. B. Photomicrograph of (A) in polarized transmitted light with a lambda filter. The annuli separating the zones are more distinctive. C. Photomicrograph of the outer cortex as indicated by bracket in (A). Vascularity has greatly decreased towards the EFS and just below the LAG. Abbreviations: EFS = external fundamental system; LAG = line of arrested growth; MC = medullary cavity.

Fig. 16. Fémur OMNH-35389 d'*O. retroversus*, longueur 221 mm. A. Scan d'une section transverse de carotte prélevée dans le côté dorsal à mi-diaphyse. Un EFS distinct peut être observé dans le cortex externe. La vascularisation est constituée de canaux longitudinaux et réticulés. Outre l'EFS, huit cycles de croissance peuvent être observés dans le cortex. Des cycles de croissance plus récents peuvent s'être résorbés. Les cavités d'érosion ne se développent pas au-delà du troisième cycle. B. Microphoto de (A) en lumière transmise polarisée avec un filtre lambda. Les annuli séparant les zones sont plus distincts. C. Microphoto du cortex externe indiqué par une équerre en (A). La vascularisation a considérablement diminué vers l'EFS et juste au-dessous de la LAG. Abréviations : EFS = système fondamental externe ; LAG = ligne de croissance arrêtée ; MC = cavité médullaire.

a possibly overlooked earliest occurrence of fibrolamellar bone in the lineage leading to mammals. Included in this sampling is Brinkman's (1988) figured *Ophiacodon* humeral growth series from RCBB. The sectioning of this ontogenetic series served two purposes: first, to answer the call for proper ontogenetic sampling of pelycosaur material as to ascertain data relevant for explaining the dense vascularity of the cortical bone. Additionally, this sample set allowed us to test Brinkman's (1988) hypothesis of morphological ontogenetic stages for a single species, *O. retroversus.* If the material represents a growth series of a single species, then histology needs to correlate with the morphologic stages of development assigned to these bones (Figs. 1 and 2).

5.1. Synthesis of histology

In general, the bone tissue of *Ophiacodon* is a mixture of WB and PFB alternating as zones and annuli. LB is restricted to the osteons and trabecular bone. The cortical bone is well vascularized. All humeri, including the Latest Carboniferous-age femur OMNH-55234 and the pre-hatching cortex of femur IPBSH-46, exhibit radially arranged longitudinal and radial canals. The organization of the canals gives the cortical bone a "bicycle wheel" pattern (see Figs. 6–10 and 15). The other femora sampled and the post-hatching cortex of IPBSH-46 show longitudinal and reticular vascular canals with varying degrees of LB infilling. True primary osteons are prevalent in all bones. A few secondary osteons were only observed in the deep cortex of the largest sampled humerus (MCZ-1486, Fig. 9F), but they are not present in the largest femur (OMNH-35389).

As confirmed by longitudinal sections (Fig. 11), osteocyte lacunae in the primary tissue of *Ophiacodon* are mostly isometric and plump (static osteocytes) whereas those that follow the circumferential layering of the LB in the osteons are basically flat (dynamic osteocytes), which is characteristic of FLB (Prondvai et al., 2014; Stein and Prondvai, 2014). The medullary cavity of the humeri is smaller and mostly occluded with secondary trabeculae in the ontogenetically older specimens, in contrast to the open MC of the femora. Mostly, the humeri and femora differ in resorption patterns, which affect the preserved growth record. In humeri, erosional cavities follow the radial organization of the vascular network and incorporate areas of primary cortical bone into the medullary region as trabeculae bound by lamellar bone. Femora completely resorb the primary cortex and develop a more open MC. Resorption and endosteal deposition seem to be occurring at a much slower rate than the periosteal deposition, resulting in a better preservation of the growth record in femora. One feature that seems consistent in the *Ophiacodon* femora, regardless of geologic age or size, is the dorsal position of the nutrient canal (Figs. 13–15). This has not yet been consistently observed in other pelycosaurs. Presence of the nutrient canal in the transverse sections reaffirms the accuracy of our sampling location, which was chosen on the premise that the minimal diaphyseal circumference (Fig. 2) is the neutral zone where growth started.

The histology of the *O. retroversus* humeral growth series does indeed correlate with the MOS assigned by Brinkman (1988) and contains histological evidence of progressive growth from a juvenile stage to fully grown adult (Figs. 4 and 5). The smallest sampled humerus MCZ-5926 (MOS II) (Table 1, Fig. 1) contains a hatching line recording the event of emergence from the amniote egg (as does the smallest femur sampled, IPBSH-46). All humeri sampled, as noted earlier, contain a highly vascularized cortex of woven and parallel-fibered bone incorporating numerous primary osteons. Through the progressive stages of growth, the medullary region expands through resorption, and secondary trabeculae form from remodeling of primary cortex. The largest humerus in the growth series, MCZ-1486 (MOSV) (Fig. 2), contains an external fundamental system, indicating that the animal had reached skeletal maturity.

However, it should be noted that humerus IPBSH-62, which also is MOS V and thus is also in the late stages of full ossification, lacks an EFS. Therefore, this animal died slightly before reaching skeletal maturity, indicating that MOS V has a lower resolution for indicating skeletal maturity than does bone histology. Another argument could be put forth with regards to the onset of the EFS identified in OMNH-73698 (MOS IV-V) as it is in the early stages of full ossification. This is consistent with the observation of Brinkman (1988) that bones of different length are classified in the same MOS (Fig. 4).

It is important to remember that these specimens, IPBSH-62 (*O. uniformis*) and MCZ-1486 (*O. retroversus*) belong to different species, which may explain the discrepancy. The same can be said for MCZ-73698 (*Ophiacodon* sp.).

In order to estimate individual age from cyclical growth marks, we need to be sure that the first preserved growth mark in the smallest humerus (MCZ-5926) and femur (IPBSH-46) is indeed a hatching line and not a later growth cycle, with the true hatching line having been resorbed. In the case of MCZ-5926, this appears rather unlikely because the primary cortical bone tissue is preserved nearly to the center of the bone cross-sections (Fig. 6A), and the only other growth marks preserved inside the presumed HL are two indistinct cycles of slowed growth, though not to the extreme as that of the HL. The presumed HL also marks the most distinctive change in bone tissue in both bones, also consistent with a major life history event such as birth (Rogers et al., 2016). Additionally, the embryonic bone inside the HL appears so highly and irregularly vascularized as well as largely or only consist of WB that the interpretation as embryonic bone appears most convincing.

The growth curve constructed from the *O. retroversus* growth series supports the hypothesis that these animals grew relatively fast compared to other pelycosaurs (Shelton, 2015) and modern squamates (Cubo et al., 2014; Laurin and de Buffrénil, 2016) (Fig. 5). This observation of fast growth is difficult to quantify further without careful body mass estimates for *Ophiacodon.* The life history of *Ophiacodon* seemingly consisted of a period of relatively fast growth followed by a period of equal or greater length, when only minimal or no growth took place. Relatively fast growth is also suggested by the nature of the growth cycle boundaries, which are mainly developed as annuli, with LAGs being only seen in the very earliest and latest cycles.

5.2. Fibrolamellar bone in Ophiacodon

Based on our sampling we can affirm that true fibrolamellar bone exists in *Ophiacodon* and that the densely vascularized woven bone is not just a simple reflection of immaturity, but was laid down during most of the entire growth period. Note that there is a change towards parallel-fibered bone near the end of life as can be observed in mature specimens (See Fig. 15D for example). Our results corroborate the original findings of Enlow and Brown (1957), Enlow (1969) and most recently Laurin and de Buffrénil (2016) that the histology of *Ophiacodon* long bones is indicative of rapid skeletal growth.

Fibrolamellar bone is defined as woven bone matrix in which the vascular canals are filled in centripetally by lamellar bone, forming primary osteons (Francillon-Vieillot et al., 1990). From an osteogenetic point of view, fibrolamellar bone is secreted by two types of osteoblasts, static and dynamic ones (Prondvai et al., 2014; Stein and Prondvai, 2014). All static osteoblasts and some of the dynamic ones differentiate into osteocytes that differ in shape. Those osteocytes that are derived from static osteoblasts are isometric ("plump") in shape, while those derived from dynamic osteoblasts are spindle-shaped. We found both types of osteocytes in *Ophiacodon* long bones (Figs. 10 and 11).

Enlow (1969) concluded that the specimen he analyzed must have been a juvenile because of the extreme difference from the other pelycosaurs; however, at the time, proper ontogenetic sampling of this group had not yet occurred in order to support this statement. De Ricqlès (1974a, p. 63) compared *Ophiacodon* cortical bone to that of therapsids, noting a similarity in the dense vascularization, but he concluded that this histology must reflect the aquatic lifestyle of *Ophiacodon*, further noting a similarity to crocodiles and plesiosaurs. While ours is not the first time that FLB has been described in pelycosaurs (see Huttenlocker and Rega, 2012; Huttenlocker et al., 2006, 2010, 2011; Shelton et al., 2013), previous studies mostly dealt with neural spines.

5.3. Intraspecific femur histovariability in O. uniformis

The *O. uniformis* femur sectioned by Laurin and de Buffrénil (2016) was described to have mostly PFB to LB tissue in the matrix. Our specimens also consisted of dominant PFB in the cortex as well as thin layers of WB but no lamellar bone. Additionally, we found secondary osteons concentrated below the nutrient canal, but Laurin and de Buffrénil (2016) stated that they did not observe them in their sample. Finally, our specimens did not contain as many LAGs in the cortex or an EFS as theirs.

5.4. Interspecific histovariability in Ophiacodon

This study looked at the bone histology of three species of *Ophiacodon*, the geologically earlier *O. mirus* and the later contemporaneous taxa *O. retroversus* and *O. uniformis*.

FLB was discovered in all species; however, it seems there was more PFB in the smallest species *O. uniformis* (particularly the femur). Vascularity of the *O. mirus* femur resembles that of a young *O. retroversus* humerus, densely organized small longitudinal and radial canals. However, *O. uniformis* seems to have the least vascularized cortex of the three species. *O. uniformis* had a higher concentration of secondary osteons in the cortex than any other species. The histological differences appear to be mostly due to species body size and not geologic age, but without proper ontogenetic sampling of *O. mirus* and *O. uniformis*, this hypothesis is speculative.

5.5. Comparison of long bone histology of Ophiacodon spp. and D. natalis

Ophiacodon is not as basal among Synapsida as once thought, but it is the sister clade to the clade consisting of Edaphosauridae, Sphenacodontidae and Therapsida (Benson, 2012; Kemp, 1987, 2007; Romer and Price, 1940). Remarkably, *Ophiacodon* histology is more reflective of fast growth than the sphenacodontid *Dimetrodon*. In sphenacodontids, there is an incipient form of FLB where osteons remain immature throughout ontogeny and the cortex contains more PFB than in *Ophiacodon* (Shelton et al., 2013). Otherwise, *Dimetrodon* and *Ophiacodon* humeri differ mainly in the patterns of resorption and remodeling in which primary bone is incorporated as trabeculae in the *Ophiacodon* MC, but in *Dimetrodon* primary bone is completely resorbed during the MC expansion process. Also, while the "bicycle wheel" vascular pattern has been described in both the humerus and femur of *Dimetrodon* (Shelton et al., 2013), it consistently only occurs in the humerus in *Ophiacodon*. Only two femora show it: the Carboniferous OMNH-55234 and the embryonic tissue of IPBSH-46. In comparison to the growth trajectory of *D. natalis* (Shelton et al., 2013, fig. 10), it is clear that *O. retroversus* reached skeletal maturity much earlier, but the life expectancy of both seems to have been similar (Fig. 5).

6. Conclusion

By sampling Brinkman's (1988) *Ophiacodon* ontogenetic series (Figs. 1 and 4), as well as additional material (Appendices 1 and 2), we have firstly shown that Brinkman's morphological stages are a reflection of ontogeny, at least for *O. retroversus*, and secondly we confirmed the presence of true fibrolamellar bone in the postcrania of pelycosaurs, which Enlow (1969) first described as "fast growing tissue". The highly vascularized cortex (which is shared by other carnivorous pelycosaurs like *Dimetrodon*) is not simply a reflection of immaturity, nor is it direct evidence for an aquatic lifestyle as was presumed by earlier studies (de Ricqlès 1974a; Romer and Price, 1940). Thus, our study does not resolve the preferred habitat of *Ophiacodon*. Isotope analysis is recommended to resolve the preferred habitat question for *Ophiacodon* (Clementz et al., 2008; Fischer et al., 2013, 2014).

Furthermore, the tissue we describe here possesses the classic histological characteristics of the textbook

definition of FLB (Francillon-Vieillot et al., 1990). In general, the compacta consist of primary osteons in a woven bone matrix. Overall, the radially vascularized FLB tissue we have described in *Ophiacodon* is more derived in terms of the osteonal development, bone matrix, and skeletal growth than what has been described thus far in any other pelycosaur, pushing back the origin of FLB in the Synapsida by 20 million years from its previous oldest occurrence in basal therapsids (Chinsamy-Turan, 2012). It is currently held that sphenacodontids are the sister group to therapsids (and not ophiacodontids) (Kemp, 1987, 2007), thus FLB in *Ophiacaodon* is probably convergently evolved with the FLB of basal therapsids (first appearing in Dinocephalia; see Reid, 1987). The lack of FLB in the basal ophiacodontid *Clepsydrops* (Laurin and de Buffrénil, 2016) strengthens the conclusion of convergent evolution of this tissue.

Funding

This project was funded by DFG grant SA 469/34-1 and the University of Bonn.

Acknowledgments

We would wholeheartedly like to thank the late Jack Loftin and his late wife Marie Loftin of Archer City, Texas, for their help and hospitality in the field. Koen Stein (Free University of Brussels) and Herman Winkelhorst (Aalten, NL) provided assistance in the field. We thank Olaf Dülfer, Rebecca Hofmann, and Marlene Nowak (all Steinmann Institute) for making the petrographic thin-sections. Yasuhisa Nakajima (Steinmann Institute), Zhe-Xi Lou (University of Chicago), and Jessica Hawthorn (University of Toronto) are thanked for discussion. Robert Reisz (University of Toronto) provided preliminary identification of the Briar Creek material. Aurore Canoville (Steinmann Institute) translated French papers, and Jessica Mitchell (Steinmann Institute) provided linguistic improvements. We thank Don Brinkman (Tyrell Museum of Palaeontology) for sharing the raw data from his 1988 study. We would like to extend our particular gratitude to the late Farish Jenkins Jr. and Jessica Cundiff (MCZ), Richard Cifelli, Jennifer Larson, and Kyle Davies (OMNH), Pamela Buzas-Stephens (MSU), and Jeffrey Wilson and Gregg Gunnell (UMMP) for access to collections and granting permission for consumptive sampling. Finally, we thank the landowner of the Briar Creek Bonebed, Jeff Lindeman, for granting permission to excavate in 2010 and 2011. We would like to thank Elizabeth Rega, Michel Laurin and Andrew Lee for constructive comments on an earlier version of this manuscript. Additionally, we would like to thank Koen Stein, Aurore Canoville, and Holly Woodward for their critique of the current manuscript.

Appendix A. Supplementary data

Supplementary data associated with this article can be found, in the online version, at doi: http://dx.doi.org/10.1016/j.crpv.2017.02.002.

References

Benson, R.B.J., 2012. Interrelationships of basal synapsids: cranial and postcranial morphological partitions suggest different topologies. J. Syst. Palaeontol. 10, 601–624.

Brinkman, D., 1988. Size-independent criteria for estimating relative age in *Ophiacodon* and *Dimetrodon* (Reptilia, Pelycosauria) from the Admiral and lower Belle Plains formations of West-central Texas. J. Vert. Paleontol. 8, 172–180.

Bybee, P.J., Lee, A.H., Lamm, E.-T., 2006. Sizing the Jurassic theropod dinosaur *Allosaurus*: assessing growth strategy and evolution of ontogenetic scaling of limbs. J. Morphol. 267, 347–359.

Case, E.C., 1915. The Permo-Carboniferous red beds of North America and their vertebrate fauna. The Carnegie Institution of Washington, Washington, DC.

Chinsamy-Turan, A.E., 2012. Forerunners of Mammals. Radiation, Histology, Biology. Indiana University Press, Bloomington, IN, USA.

Clementz, M.T., Holroyd, P.A., Koch, P.L., 2008. Identifying aquatic habits of herbivorous mammals through stable isotope analysis. Palaios 23, 574–585.

Cubo, J., Baudin, J., Legendre, L., Quilhac, A., de Buffrénil, V., 2014. Geometric and metabolic constraints on bone vascular supply in diapsids. Biol. J. Linn. Soc. 112, 668–677.

Currey, J.D., 2002. Bones. Structure and Mechanics. Princeton University Press, Princeton, NJ, USA.

Enlow, D.H., 1969. The bone of reptiles. In: Gans, C. (Ed.), Biology of the Reptiles Morphology, Vol. 1. Academic Press, pp. 45–80.

Enlow, D.H., Brown, S.O., 1957. A comparative histological study of fossil and recent bone tissues. Part II. Texas J. Sci. 9 (2), 186–214.

Enlow, D.H., Brown, S.O., 1958. A comparative histological study of fossil and recent bone tissues. Part III. Texas J. Sci. 10 (2), 187–230.

Fischer, J., Schneider, J.W., Hodnett, J.M., Elliott, D.K., Johnson, G.D., Voigt, S., Joachimski, M.M., Tichomirowa, M., Götze, J., 2014. Stable and radiogenic isotope analyses of shark teeth from the Early to the Middle Permian (Sakmarian-Roadian) of the southwestern USA. Hist. Biol. 2, 710–727.

Fischer, J., Schneider, J.W., Voigt, S., Joachimski, M.M., Tichomirowa, M., Tütken, T., Götze, J., Berner, U., 2013. Oxygen and strontium isotopes from fossil shark teeth: environmental and ecological implications for Late Palaeozoic European basins. Chem. Geol. 342, 44–62.

Francillon-Vieillot, H., de Buffrénil, V., Castanet, J., Géraudie, F., Meunier, F.J., Sire, J.Y., Zylberberg, L., de Ricqlès, A., 1990. Microstructure and mineralization of vertebrate skeletal tissues. In: Carter, J.G. (Ed.), Skeletal Biomineralization: Patterns, Processes and Evolutionary Trends, Vol. 1. Van Nostrand Reinhold, New York, pp. 471–530.

Germain, D., Laurin, M., 2005. Microanatomy of the radius and lifestyle in amniotes (Vertebrata, Tetrapoda). Zool. Scripta 34, 335–350.

Hentz, T.F., 1988. Lithostratigraphy and paleoenvironments of Upper Paleozoic continental red beds, north-central Texas: Bowie (new) and Wichita (revised) groups. University of Texas at Austin, Bur. Econ. Geol., Rep. Inv. 17, 1–55.

Huttenlocker, A., Rega, E., 2012. The paleobiology and bone microstructure of pelycosaurian-grade synapsids. In: Chinsamy, A. (Ed.), Forerunners of Mammals. Radiation, Histology, Biology. Indiana University Press, Bloomington, IN, USA, pp. 9–119.

Huttenlocker, A., Angielczyk, K.D., Lee, A., 2006. Osteohistology of *Sphenacodon* (Synapsida: Sphenacodontidae) and the hidden diversity of growth patterns in basal synapsids. J. Vert. Paleontol. 26 (Supplement to Issue 3), 79–80A.

Huttenlocker, A., Mazierski, D., Reisz, R., 2011. Comparative osteohistology of hyper-elongate neural spines in Edaphosauridae (Amniota: Synapsida). Palaeontology 54, 573–590.

Huttenlocker, A., Rega, E., Sumida, E.S., 2010. Comparative anatomy and osteohistology of hyperelongate neural spines in the sphenacodontids *Sphenacodon* and *Dimetrodon* (Amniota: Synapsida). J. Morphol. 27, 1407–1421.

Kemp, T.S., 1987. Mammal-like reptiles and the origin of mammals. Academic Press, London.

Kemp, T.S., 2007. The origin and evolution of mammals. Oxford University Press, Oxford, UK.

Kissel, R.A., Lehman, T.M., 2002. Upper Pennsylvanian tetrapods from the Ada Formation of Seminole County, Oklahoma. J. Paleont. 76, 529–545.

Klein, N., Sander, P.M., 2007. Bone histology and growth of the prosauropod *Plateosaurus engelhardti* Meyer, 1837 from the Norian bonebeds of Trossingen (Germany) and Frick (Switzerland). Palaeontology 77, Spec. Pap., 169–206.

Laurin, M., de Buffrénil, V., 2016. Microstructural features of the femur in early ophiacodontids: a reappraisal of ancestral habitat use and lifestyle of amniotes. C. R. Palevol 15 (1–2), 119–131.

Marsh, O.C., 1878. Notice of new fossil reptiles. Am. J. Sci. 89, 409–411.
May, W., Huttenlocker, A., Pardo, J.D., Benca, J., Small, B.J., 2011. New Upper Pennsylvanian armored dissorophid records (Temnospondyli, Dissorophoidea) from the U.S. midcontinent and the stratigraphic distributions of dissorophids. J. Vert. Paleontol. 31, 907–912.
Nopcsa, F., 1923. Die Familien der Reptilien. Fortschritte der Geologie und Paläontologie 2, 1–210.
Olson, E.C., 1967. Early Permian vertebrates of Oklahoma. Oklahoma Geol. Surv. Cir. 74, 1–107.
Olson, E.C., 1977. Permian lake faunas: a study in community evolution. J. Palaeontology Soc. India 20, 146–163.
Petermann, H., Sander, P.M., 2013. Histological evidence for muscle insertion in extant amniote femora: implications for muscle reconstruction in fossils. J. Anat. 222 (4), 419–436.
Prondvai, E., Stein, K., de Ricqlès, A., Cubo, J., 2014. Development-based revision of bone tissue classification: the importance of semantics for science. Biol. J. Linn. Soc. 112, 799–816.
Reid, R.E.H., 1987. Bone and dinosaurian "endothermy". Mod. Geol. 11 (2), 133–154.
Reisz, R.R., 1986. Encyclopedia of Paleoherpetology. Part 17A: Pelycosauria. Gustav Fischer Verlag, Stuttgart.
Ricqlès, A. de., 1972. Recherches paléohistologiques sur les os longs des tétrapodes, III. – Titanosuchiens, Dinocéphales et Dicynodontes. Ann. Paleontol. 58, 17–60.
Ricqlès, A. de., 1974a. Evolution of endothermy: histological evidence. Evol. Theory 1, 51–80.
Ricqlès, A. de., 1974b. Recherches paléohistologiques sur les os longs des Tétrapodes IV.– Éothériodontes et Pélycosaures. Ann. Paleontol. 60, 3–39.
Rogers, K.C., Whitney, M., D'Emic, M., Bagley, B., 2016. Precocity in a tiny titanosaur from the Cretaceous of Madagascar. Science 352, 450–453.
Romer, A.S., 1956. Osteology of the reptiles. The University of Chicago Press, Chicago.
Romer, A.S., 1974. The stratigraphy of the Permian Wichita redbeds of Texas. Breviora 427, 1–31.
Romer, A.S., Price, L.W., 1940. Review of the Pelycosauria. Geol. Soc. Am., Spec. Pap. 28, 1–538.
Sander, P.M., 1989. Early Permian depositional environments and pond bonebeds in central Archer County, Texas. Paleobiogeogr., Palaeoclimatol., Palaeoecol. 69, 1–21.
Sander, P.M., Klein, N., 2005. Developmental plasticity in the life history of a prosauropod dinosaur. Science 310, 1800–1802.
Sander, P.M., Mateus, O., Laven, T., Knötschke, N., 2006. Bone histology indicates insular dwarfism in a new Late Jurassic sauropod dinosaur. Nature 441, 739–741.
Shelton, C., Sander, P.M., Stein, K., Winkelhorst, H., 2013. Long bone histology indicates sympatric species of *Dimetrodon* (Lower Permian, Sphenacodontidae). Earth Env. Sci. Trans. R. Soc. Edinburgh 103 (3–4), 217–236.
Shelton, C.D., (Ph.D. Dissertation) 2015. Origins of Endothermy in the Mammalian Lineage: the Evolutionary Beginning of Fibrolamellar Bone in the "Mammal-Like" Reptiles. Rheinische Friedrich-Wilhelms-Universität Bonn, Bonn, Germany.
Stein, K., Prondvai, E., 2014. Rethinking the nature of fibrolamellar bone: an integrative biological revision of sauropod plexiform bone formation. Biol. Rev. 89, 24–47.
Stein, K., Sander, P.M., 2009. Histological core drilling: a less destructive method for studying bone histology. Methods in fossil preparation. In: Brown, M.A., Kane, J.F., Parker, W.G. (Eds.), Proceedings of the first annual Fossil Preparation and Collections Symposium. , pp. 69–80 (ISBN 1-11111-111-1).